Title	液相エピタキシーによるCaAsおよび関連混晶の成長
Author(s)	土居，功年
Citation	大阪大学，1979，博士論文
Version Type	VoR
URL	https://hdl.handle.net/11094/1979
rights	
Note	

GROWTH OF GaAs AND RELATED ALLOYS BY LIQUID PHASE EPITAXY

Atsutoshi Doi

Central Research Laboratory, Hitachi Ltd.,

Kokubunji, Tokyo

Growth of GaAs and Related Alloys by Liquid Phase Epitaxy

Atsutoshi Doi

Central Research Laboratory, Hitachi Ltd.,
Kokubunji, Tokyo

ABSTRACT

Liquid phase epitaxy (LPE) of thin GaAs layers is investigated both experimentally using a horizontal sliding boat and theoretically assuming that the growth process is diffusion controlled. The excellent agreement between calculated and experimental results indicates that the diffusion limited growth model is valid for expressing the growth process in the LPE. It is found that the thickness of the GaAs epitaxial layer can be controlled by the following five growth parameters : initial temperature, initial supercooling, cooling rate, solution thickness, and growth duration.

An improved LPE technique is developed. In this technique, a dummy crystal is introduced to control the initial supercooling, which is nearly uncontrollable in the previous technique. Reproducible growth of submicron GaAs multiple layers is possible using the new LPE technique.

The analysis of the LPE of the binary Ga-As system is extended to the ternary Ga-Al-As system. The influence of various growth conditions on crystal composition in the GaAlAs epitaxial layer and on epitaxial layer thickness is investigated in detail. It is shown that uniform AlAs mole fraction profile can be obtained by controlling the following growth conditions : cooling rate, solution thickness, and initial supercooling. The dependences of the GaAlAs layer thickness on growth conditions are similar to those of GaAs except for a factor which depends on the AlAs mole fraction.

Compound semiconductor LPE has been successfully applied to the fabrication of transfered electron oscillator diodes, double-drift region IMPATT diodes, MESFET's, and injection lasers. The LPE crystals are shown to meet the respective specifications and provide excellent device performances.

TABLE OF CONTENTS

Page

1. INTRODUCTION

Liquid phase epitaxy (LPE) is becoming a widely used technique for growing high-quality III-V semiconductors and related alloys. It has been successfully applied to the fabrication of electroluminescent diodes1), laser diodes2), and high-frequency devices such as transferred electron oscillator diodes3) and IMPATT diodes4,5).

From the applicational point of view, the following properties of grown layers are of greatest significance : layer thickness, uniformity of thickness, crystal composition, compositional profile, carrier concentration, carrier concentration profile through the layer, and surface morphology. To control the quality of the grown layers in terms of structural compositional, electrical, and morphological perfection, many experiments have been done, and successful achievements in controlled growth have been reported6-19). However, it is still very difficult to control the layer thickness to less than 0.5 μm under most growth conditions. This is largely due to a lack of fundamental data and knowledge about the physical processes occurring during LPE.

The first aim of this work is to investigate a new LPE method for growing thin GaAs layers both theoretically and experimentally. Most studies[20-26) deal with LPE using a solution sufficiently thick as to be considered infinite. But in LPE, it is difficult to control the epitaxial layer thickness to less than 0.5 μm. Recently, some LPE techniques useful for growing thin epitaxial layers have been reported elsewhere[1,27-29), but the influence of the growth parameters on the layer thickness has not been sufficiently clarified.

In this work, the solution thickness was reduced to be less than the diffusion length of As[30). Moreover, a dummy crystal was introduced to control the supercooling[31) on the top surface of the thin Ga solution. The growth process has been analyzed assuming that the growth rate is diffusion controlled. It is shown that the experimental results agree well with the calculated results, and that the diffusion limited growth model is a good approximation for the LPE of GaAs. The epitaxial layer thickness was controlled by the following five growth parameters : initial temperature, initial supercooling, cooling rate, solution thickness and growth duration. The reproducible growth of submicron GaAs multiple layers was achieved by controlling the initial supercooling.

The second aim is to extend the analysis of the LPE of the binary Ga-As system to the ternary Ga-Al-As system. The influence of growth conditions on the AlAs mole fraction in the GaAlAs epitaxial layer as well as the layer thickness has been investigated in detail. It is shown that a uniform AlAs mole fraction can be obtained by an appropriate choice of growth conditions : cooling rate, solution thickness, and initial supercooling. The dependences of the layer thickness on the growth conditions are similar to those of GaAs except for a factor which depends on the AlAs mole fraction.

The quality of the LPE layers has been examined by fabricating injection lasers and high-frequency devices such as transferred electron oscillator (TEO) diodes, double-drift region IMPATT diodes, and MESFET's. It was found that the structural, compositional and electrical qualities were successfully controlled to meet device specifications.

This thesis is composed of six chapters. In the next chapter, a detailed theoretical analysis of the

LPE of GaAs is given. The calculated results are compared with the experimental results in Chapter 3. The analysis is extended to the GaAlAs ternary system in Chapter 4. Applicational examples to microwave devices and laser diodes are given in Chapter 5. The conclusions of this work are summarized in Chapter 6.

2. DIFFUSION LIMITED GROWTH THEORY

2.1 Diffusion Limited Growth Model

It has been pointed out that bulk transport processes and interface kinetics play an important role in solution growth. It is generally understood that the term 'bulk transport processes' includes transport by convection, stirring, and diffusion. And the term 'interface kinetics' includes processes such as adsorption and desorption, dissociation and chemical reaction, migration, capture at growth sites, nucleation and the production of active growth sites. Various theories which take these factors into account have been reported20-22,26,32-34). In this paper, only the transport process by diffusion has been taken into account to obtain relations between the epitaxial layer thickness and growth parameters. Though this is a simple model, the calculated results give very good agreement with the experimental results which will be described in the following chapter.

The assumptions used in this theoretical treatment are as follows :

1) The crystal surface is planar. Therefore, there is no lateral solute flow and no variation of freezing point, both of which would occur at a curved solid-liquid interface. This assumption makes it sufficient to consider the one-dimensional diffusion problem.

2) The solution and substrate are isothermal. The heat of fusion evolved at the solid-liquid interface and the heat transfer away from the solution are not taken into account, because the thermal diffusion coefficient is higher by about four orders of magnitude than the diffusion coefficient of the solute.

3) The liquid and solid are in equilibrium at the interface35). The interface kinetics are assumed to be fast enough not to be the rate-limiting step.

4) The solid-liquid interface moves at the speed of the growth rate. But this movement is neglected because only a thin layer growth is considered.

5) The diffusion coefficient of As in Ga solution is 5×10^{-5} cm^2/sec30) at 744 °C.

6) The critical supercooling is 6 °C30).

The validity of assumptions 5 and 6 is discussed in detail in the following chapter.

Solute concentration distribution in the solution is shown schematically in Fig. 1. At the solid-liquid

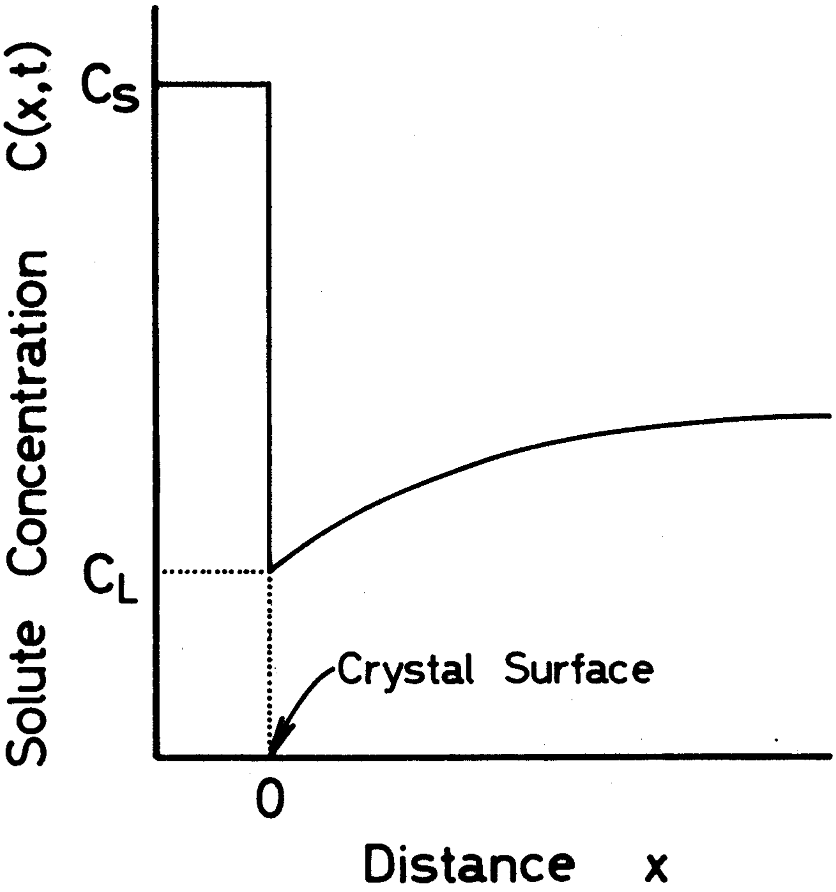

Fig. 1. Solute concentration distribution in the solution.

interface, the solute concentration $C(x,t)$ is equal to the equilibrium concentration $C_L(T)$. In the regions away from the interface, the solution is in a state of thermodynamic nonequilibrium. The resulting concentration gradient leads to solute transfer. The driving force for the diffusion is provided, for example, by a temperature gradient or a temperature change. In this model, the growth rate is assumed to be limited by the solute diffusion. Thus the one-dimensional diffusion equation to be solved is

$$D \frac{\partial^2 C}{\partial x^2} = \frac{\partial C}{\partial t} , \qquad .....(1)$$

where D is the diffusion coefficient of As in the Ga solution.

The boundary condition at the solid-liquid interface is

$$C(0,t) = C_L(T). \qquad .....(2)$$

The equilibrium As concentration is given by the phase diagram36-38) and represented as follows24),

$$C_L(T) = K \exp(-\Delta H/R_0 T), \qquad .....(3)$$

where ΔH is the heat of solution, R_0 the gas constant, and K a constant. Equation (3) gives good agreement with the Ga-As liquidus line in the Ga-rich region for $K=2.19\times10^{26}$ cm^{-3} and $\Delta H/R_0=1.32\times10^4$ degrees. When the temperature is lowered at a constant rate a, the temperature is given by

$$T(t) = T_0 - at, \qquad .....(4)$$

where T_0 is initial temperature. Then Eq. (3) can be approximated in the form,

$$C_L(T) = C_0 \exp(-t/\tau), \qquad .....(5)$$

where C_0 is the equilibrium concentration at the initial temperature T_0, and $1/\tau=\Delta H\ a\ R_0^{-1}\ T_0^{-2}$. This approximation is valid when $at/T_0 \ll 1$.

The initial condition and the other boundary condition depend on the methodology and geometry of the LPE. In the following section, the boundary conditions corresponding to various LPE techniques are explained in detail.

The growth rate can be expressed by the following relation which is required by mass conservation in the solid-liquid interface region :

$$R = \frac{D\left(\frac{\partial C}{\partial x}\right)_{x=0}}{C_s - C(0,t)} \quad , \qquad \text{.....(6)}$$

where R is the growth rate and C_s the As concentration in the crystal. Since $C_s \gg C(0,t)$ in the growth from dilute solution, we can write

$$R = \frac{D\left(\frac{\partial C}{\partial x}\right)_{x=0}}{C_s} \qquad \text{.....(7)}$$

and the thickness of the epitaxial layer grown in a time period t is

$$G = \int_0^t R \; dt \; . \qquad \text{.....(8)}$$

Thus we can obtain the growth rate and layer thickness by solving Eq. (1) and substituting it into Eqs. (7) and (8).

2.2 Theoretical Analysis of GaAs LPE

2.2.1 General case

The As concentration profile and the temperature distribution in the solution are shown in Fig. 2. In the general case of GaAs LPE, there may be three kinds of driving forces for the solute diffusion : initial supercooling, temperature lowering, and temperature gradient.

When the solution is saturated at $T_0 + \Delta T$, the As concentration profile is uniform in the solution and the concentration is equal to $C_0 + \Delta C$. The epitaxial growth is started at T_0 by the step cooling. The excess As concentration ΔC is the initial supercooling, and C_0 is the equilibrium concentration at the initial temperature T_0. Thus the initial condition is given by

$$C(x,0) = C_0 + \Delta C \ . \qquad \text{.....(9)}$$

One of the boundary condition is given by Eq. (5), which expresses the driving force due to temperature lowering. When the source crystal is placed at

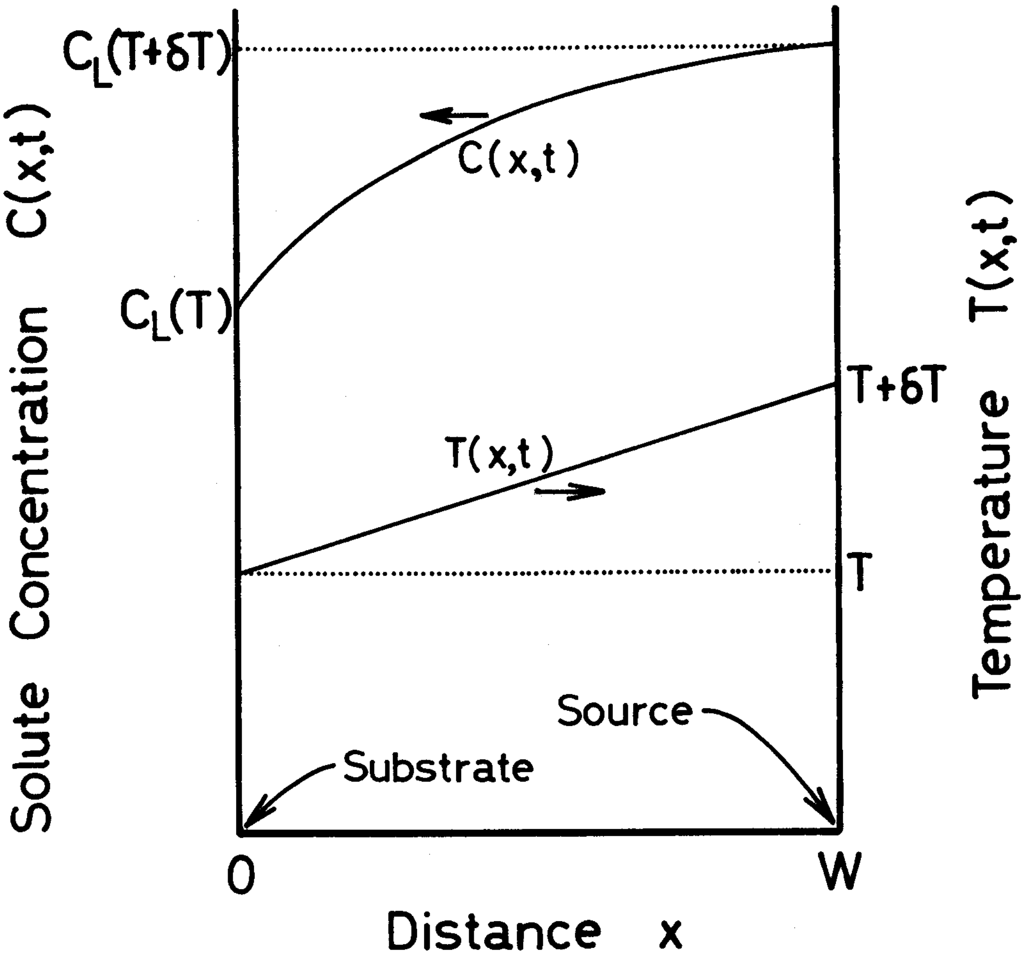

Fig. 2. As concentration and temperature distribution in the solution.

x=W, and the temperature gradient $\delta T/W$ is applied to the solution, the other boundary condition is given by

$$C(W,t) = (C_0 + \delta C)\ \exp(-t/\tau)\ , \qquad \ldots\ldots(10)$$

where $C_0 + \delta C = C_L(T_0 + \delta T)$.

If there is no homogeneous nucleation in the Ga solution, the As concentration profile in the solution, the growth rate, and the epitaxial layer thickness can be calculated from the following equations :

$$C(x,t) = \frac{\Delta C}{\varepsilon_n^2}\frac{4D}{W^2}\ (2n+1)\ \pi\ \sin\frac{(2n+1)\pi x}{W}\ \exp(-\varepsilon_n^2\ t)$$

$$+\ C_0\left[\ \frac{\alpha\ \sin\frac{x}{\lambda} + \sin(\theta - \frac{x}{\lambda})}{\sin\ \theta}\ \exp(-t/\tau)\right.$$

$$+ \sum\frac{2Dn\pi}{W^2}\ \sin\frac{n\pi x}{W}\ \left(\frac{1}{\frac{1}{\tau} - \omega_n^2} + \frac{1}{\omega_n^2}\right)$$

$$\left. -(-1)^n\ \left(\frac{\alpha}{\frac{1}{\tau}-\omega_n^2} + \frac{1}{\omega_n^2}\right)\ \exp(-\omega_n^2\ t)\right]\ ,$$

$$\ldots\ldots(11)$$

$$R(t) = \frac{4D\ \Delta C}{C_s\ W} \sum \exp(-\varepsilon_n^2\ t) + \frac{D\ C_0}{C_s\ W} \Bigg[\theta\ \frac{\alpha-\cos\theta}{\sin\theta}\ \exp(-t/\tau)$$

$$+2 \sum \omega_n^2 \quad \left(\frac{1}{\frac{1}{\tau}-\omega_n^2} + \frac{1}{\omega_n^2} \right) - (-1)^n \left(\frac{\alpha}{\frac{1}{\tau}-\omega_n^2} + \frac{1}{\omega_n^2} \right)$$

$$\exp(\ -\ \omega_n^2\ t\ ) \Bigg] \ , \qquad .....(12)$$

$$G(t) = \frac{4D\ \Delta C}{C_s\ W} \sum \frac{1-\exp(-\varepsilon_n^2\ t)}{\varepsilon_n^2} + \frac{D\ C_0}{C_s\ W} \Bigg[\tau\ \ \theta\ \frac{\alpha-\cos\theta}{\sin\theta}$$

$$\Big\{ 1-\exp(-t/\tau) \Big\} + 2 \sum \Bigg\{ \left(\frac{1}{\frac{1}{\tau}-\omega_n^2} + \frac{1}{\omega_n^2} \right)$$

$$-(-1)^n \left(\frac{\alpha}{\frac{1}{\tau}-\omega_n^2} + \frac{1}{\omega_n^2} \right) \Bigg\} \Big\{ 1\ -\ \exp(-\omega_n^2\ t) \Big\} \Bigg] \ ,$$

$$.....(13)$$

where $\lambda=(D\tau)^{1/2}$, $\theta=W/\lambda$, $\alpha=(C_0+\delta C)/C_0$, $\varepsilon_n^2=D\left\{(2n+1)\pi/W\right\}^2$, and $\omega_n^2=D(n\pi/W)^2$. The first terms in Eqs.(11), (12), and (13) show the contributions from the initial supercooling.

2.2.2 The effect of the temperature gradient

The magnitude of the contribution from the temperature gradient is investigated in detail. When the temperature gradient normal to the solid-liquid interface is the only driving force for solute diffusion, the As concentration profile, growth rate, and layer thickness are

$$C(x,t) = C_0 + \frac{x}{W}\frac{\delta C}{} + \sum(-1)^n \frac{2Dn\pi}{W^2}\frac{\delta C}{\omega_n^2} \sin\frac{n\pi x}{W}\exp(-\omega_n^2 t), \qquad \text{.....(14)}$$

$$R(t) = \frac{D}{C_s}\frac{\delta C}{W}\left\{1 + 2\sum(-1)^n \exp(-\omega_n^2 t)\right\}, \qquad \text{..(15)}$$

$$G(t) = \frac{D}{C_s}\frac{\delta C}{W}\left[t + 2\sum\frac{(-1)^n}{\omega_n^2}\left\{1 - \exp(-\omega_n^2 t)\right\}\right]. \qquad \text{.....(16)}$$

These equations are the limiting case for $C \rightarrow 0$ and $a \rightarrow 0$ in Eqs. (11), (12), and (13). In the steady state, the growth rate is

$$R = \frac{D\ \delta C}{C_s\ W} . \qquad \text{.....(17)}$$

An approximate equation for δC can be obtained from Eq.(3) with the assumption that $\Delta H \delta T/(R_0 T_0{}^2)^{-1} \ll 1$, namely

$$\delta C = \frac{C_0\ \Delta H}{R_0\ T_0^2}\ \delta T . \qquad \text{.....(18)}$$

With Eqs. (17) and (18), the steady state growth rate and layer thickness corresponding to the temperature gradient are found to be

$$R = \left(\frac{C_0\ \Delta H\ D}{T_0^2\ R_0\ C_s} \right) \left(\frac{\delta T}{W} \right) , \qquad \text{.....(19)}$$

$$G(t) = \left(\frac{C_0\ \Delta H\ D}{T_0^2\ R_0\ C_s} \right) \left(\frac{\delta T}{W} \right) t . \qquad \text{.....(20)}$$

The layer thickness varies linearly with time t and the temperature gradient $(\delta T/W)$ in the steady state. The magnitude of the growth rate can be estimated by substituting an appropriate numerical value for Ga-As systems into Eq. (19) :

$$R = 1.4 \times 10^{-2} \left(\frac{\delta T}{W} \right) \quad (\mu m/min) \qquad .....(21)$$

at 790 °C. As the growth rate is generally ~1 μm/min when the driving force is provided by the temperature lowering or initial supercooling, the effect of the temperature gradient on layer thickness can be neglected in the temperature lowering LPE technique or in the step cooling LPE method when the temperature gradient is less than 1 °C/cm.

2.2.3. The effect of the temperature lowering

When there is no temperature gradient and no initial supercooling, i.e., when the temperature lowering is the only driving force, the As concentration distribution, growth rate, and layer thickness are given by

$$C(x,t) = C_0 \left\{ \frac{\cos(\frac{x}{\lambda} - \frac{\theta}{2})}{\cos \frac{\theta}{2}} \exp(-t/\tau) \right.$$

$$+\sum \frac{4D(2n+1)}{W^2} \left(\frac{1}{\frac{1}{\tau} - \varepsilon_n^2} + \frac{1}{\varepsilon_n^2} \right)$$

$$\sin \frac{(2n+1)\pi x}{W} \exp(-\varepsilon_n^2 t) \Big] , \qquad .....(22)$$

$$R(t) = \frac{D C_0}{C_s W} \Big[\theta \tan \frac{\theta}{2} \exp(-t/\tau)$$

$$+4\sum \varepsilon_n^2 \left(\frac{1}{\frac{1}{\tau} - \varepsilon_n^2} + \frac{1}{\varepsilon_n^2} \right) \exp(-\varepsilon_n^2 t) \Big], \qquad .....(23)$$

$$G(t) = \frac{D C_0}{C_s W} \Big[\tau\theta \tan \frac{\theta}{2} \left\{ 1 - \exp(-t/\tau) \right\}$$

$$+4\sum \left(\frac{1}{\frac{1}{\tau} - \varepsilon_n^2} + \frac{1}{\varepsilon_n^2} \right) \left\{ 1 - \exp(-\varepsilon_n^2 t) \right\} \Big] . \qquad .....(24)$$

These equations are the limiting case for $\Delta C \to 0$ and $\delta C \to 0$ in Eqs. (11), (12), and (13). When the solution thickness is thin enough, i.e. $(Dt)^{1/2} \gg W$, a simple equation for the layer thickness can be derived from Eq. (24) :

$$G(t) = \frac{1}{2} \left(\frac{\Delta H \ K}{R_0 \ C_s} \right) \left(\frac{\exp\left(-\frac{\Delta H}{R_0 T_0}\right)}{T_0^2} \right) W \cdot a \cdot t. \qquad ....(25)$$

This equation shows that the layer thickness can be decreased by decreasing the solution thickness. This LPE method is very suitable for the growth of thin layers and will be discussed in Chapter 3.

2.2.4. Liquid phase epitaxy from thin solution

In the LPE technique described in the above sections, the source crystal is placed on the top surface of the solution. When the source crystal is not introduced, the As concentration in the solution, the growth rate, and the epitaxial layer thickness can be calculated from the following equations :

$$C(x,t) = \frac{4\ \Delta C}{\pi} \sum (-1)^n \frac{\cos\left\{\frac{2n+1}{2}\pi(W-x)/W\right\}}{2n+1} \exp(-\lambda_n^2\ t/\tau) + C_0 \left[\frac{\cos\ (W-x)/\lambda}{\cos(W/\lambda)} \exp(-t/\tau) - \frac{4}{\pi} \sum (-1)^n \frac{\exp(\lambda_n^2\ t/\tau)}{\lambda_n^2 - 1} \frac{\cos\left\{\frac{2n+1}{2}\pi\ (W-x)/W\right\}}{2n+1}\right], \quad .....(26)$$

$$R(t) = \frac{2D\ \Delta C}{C_s\ W} \sum \exp(-\lambda_n^2\ t/\tau) + \frac{D\ C_0}{C_s\ W} \left[\exp(-t/\tau)\ \theta \tan\theta - \sum \frac{2}{\lambda_n^2 - 1} \exp(-\lambda_n^2\ t/\tau)\right], \quad ....(27)$$

$$G(t) = \frac{8\ \Delta C\ W}{\pi^2\ C_s} \sum \frac{1 - \exp(-\lambda_n^2\ t/\tau)}{(2n+1)^2}$$

$$+\frac{C_0 W}{C_s}\left[\frac{\tan\theta}{\theta}\left\{1 - \exp(-t/\tau)\right\}\right.$$

$$\left.-\frac{2}{\theta^2}\sum\frac{1-\exp(-\lambda_n^2\ t/\tau)}{\lambda_n^2\ (\lambda_n^2 - 1)}\right], \qquad .....(28)$$

where $\lambda_n = \frac{1}{2}(2n + 1)\pi(1/\theta)$. These equations are derived in the same manner as those in Section 2.2.1 using the boundary conditions

$$C(x,0) = C_0 + \Delta C,$$

$$C(0,t) = C_0 \exp(-t/\tau),$$

$$\left(\frac{\partial C}{\partial x}\right)_{x=W} = 0.$$

The functional relationship of the epitaxial layer thickness to the growth parameters is not discernible in Eq. (28) because Eq. (28) involves an infinite series. Equation (28) can be simplified by using the Euler summation formula for the two limiting cases $(Dt)^{1/2} \gg W$ and $(Dt)^{1/2} \ll W$:

$$G(t) = \frac{\Delta H\ K}{R_0\ C_s}\left[T_0^{-2}\exp\left(-\frac{\Delta H}{R_0\ T_0}\right)\right] W\ (\Delta T + at), \qquad .....(29)$$

for $(Dt)^{1/2} \gg W$;

$$G(t) = 2\frac{\Delta H}{R_0}\frac{K}{C_s}\left(\frac{D}{\pi}\right)^{1/2} T_0^{-2}\exp\left(-\frac{\Delta H}{R_0 T_0}\right) \quad (\Delta T t^{1/2}+\tfrac{2}{3}at^{3/2}) \qquad \ldots\ldots(30)$$

for $(Dt)^{1/2} \ll W$, where ΔT is the initial supercooling expressed as temperature.

The common factor $T_0^{-2}\exp(-\Delta H/R_0T_0)$ in Eqs. (29) and (30) shows the temperature dependence of the epitaxial layer thickness on the initial growth temperature. The first terms in Eqs. (29) and (30) show the effect of initial supercooling on the layer thickness. The second term in Eq. (30) is equivalent to the result obtained by Small and Barnes20). When the Ga solution is finite, only a finite layer can be grown. The maximum thickness of the epitaxial layer is given by

$$G = \frac{C(i)-C(f)}{C_s} W , \qquad \ldots\ldots(31)$$

where C(i) and C(f) are the equilibrium As concentration in the solution at temperature $T_0 + \Delta T$ and $T_0 - at$, respectively. It can be easily shown that Eq. (29) is equivalent to Eq. (31), that is, almost all of the excess As atoms deposit onto the substrate when $(Dt)^{1/2} \gg W$.

It is also shown by Eq. (29) that the thin Ga solution is desirable for the growth of thin layers. By comparing Eq. (25) and the second term of Eq. (29), it is seen that the thickness of the epitaxial layer in a given growth time can be halved by using a dummy crystal on the top surface of the solution.

2.2.5. Numerical calculations

Numerical method have also been applied to analyze the liquid phase epitaxy of GaAs in Ga solution. In this method, it is possible to take into account the complex boundary conditions such as the exact temperature program, homogeneous nucleation in Ga solution at critical supercooling, and the existence of stirring.

It is well known that solubility increases as the size of the source crystal decreases. The solubility is related to the particle radius by the Ostwald-Freundlich equation[39],

$$\ln \frac{C_1}{C_2} = \frac{2M\sigma}{R_0 T\rho} \left(\frac{1}{r_1} - \frac{1}{r_2}\right), \qquad .....(32)$$

where C_1 and C_2 are the solubilities of particles with radii r_1 and r_2, respectively, R the gas constant, T the temperature, ρ the density of the solid, M the molecular weight of the solid in solution, and σ the surface energy of the solid particles in in contact with the solution. In conformity with this solubility increase, there is no creation of small crystalline particles in the supercooled solution when the supercooling is less than a critical value. In other words, the solution can support a certain degree of supercooling without causing homogeneous nucleation. If the As concentration exceeds a critical value at a distance x_c away from the solid-liquid interface, homogeneous nucleation starts and the difference between C(x,t) and $C_L(T(t))$ is kept at a value ΔC_c :

$C(x,t) = C_L(T(t)) + \Delta C_c = C_L(T(t) + \Delta T_c)$, for $x \geq x_c$ and $(\frac{\partial C}{\partial x})_{x=x_c} = 0$, where ΔT_c is the critical supercooling.

If there is stirring by convection, the diffusion takes place through a narrow boundary layer adjacent to the solid-liquid interface. In the stirred region of the solution, uniform As concentration is assumed.

3. CALCULATED RESULTS AND EXPERIMENTAL EVIDENCES FOR THE LIQUID PHASE EPITAXY OF GaAs

3.1. Growth Apparatus and Procedure for Single-Layer Growth

There are several types of LPE growth apparatus : the tipping system40), the dipping system41,42), the rotating system6,43), and the sliding boat system2,44). In this work, a horizontal sliding boat was used to grow the GaAs layers. A cross-sectional view of the boat which was used for single layer growth is shown in Fig. 3. The upper part of the Ga solution was moved by pulling a quartz rod and slider 1, and the thickness of the remaining Ga solution was made equal to that of slider 2. The thickness of the solution was varied in the range 0.25-10 mm by varying the thickness of slider 2.

A GaAs (100)-oriented substrate (Sn doped, $n=1.5\times10^{18}$ cm^{-3}) was used for the epitaxial growth just after chemical etching by a mixed solution of H_2SO_4, H_2O_2, and H_2O. The boat was placed in a uniform temperature zone (± 0.5 °C) in a horizontal furnace using Pd-purified hydrogen as the atmosphere

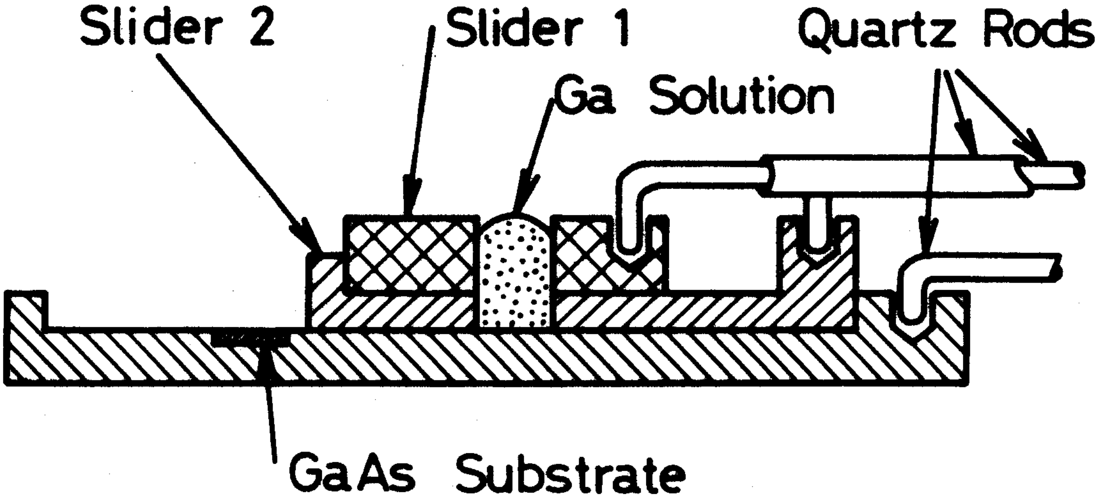

Fig. 3. Cross-sectional view of horizontal sliding boat for LPE of thin GaAs layer.

gas. No temperature gradient was detected in this furnace.

Initially, the boat was heated to a temperature 0 to 30 °C above the initial growth temperature (744 °C) and maintained at that temperature for 30 min in order to ensure the homogeneity of the Ga-As solution. Then slider 1 was moved in order to form a thin Ga solution and remove the excess GaAs source floating on the solution. The furnace then was cooled at a constant rate of 2.4 °C/min and the thin solution was moved onto the horizontal substrate at 744 °C. That is, epitaxial growth of GaAs was started at 744 °C using the thin Ga solution with initial supercooling of 0 to 30 °C. After a specified time, the solution was rapidly removed.

The epitaxial wafer was then cleaved and the cleaved surface was stained to show the interface between the substrate and the epitaxial layer. The thickness of the GaAs epitaxial layer was measured using an optical microscope.

3.2. Results and Discussion for Single Layer Growth

3.2.1. The effect of the solution thickness

The epitaxial layer thickness is plotted against the thickness of the Ga solution for growth durations of 340, 925, and 1800 sec in Fig. 4. The growth conditions used are as follows : initial supercooling, 0 °C ; initial growth temperature, 744 °C ; and cooling rate, 2.4 °C/min. The error-bars in the plot show the lateral variation of the layer thickness. The solid lines show the calculated values for the case where the effect of homogeneous nucleation was taken into account, while the broken lines show the values for the case where the effect was neglected.

As shown in this graph, when the thickness of the solution is more than 1.2 mm, the thickness of the epitaxial layer is independent of that of the solution and there are differences between the solid and broken lines, except for when the growth duration is 340 sec. This is because the epitaxial layer thickness is influenced considerably by homogeneous nucleation which starts about 1.2 mm away from the solid-liquid interface. This will be explained in

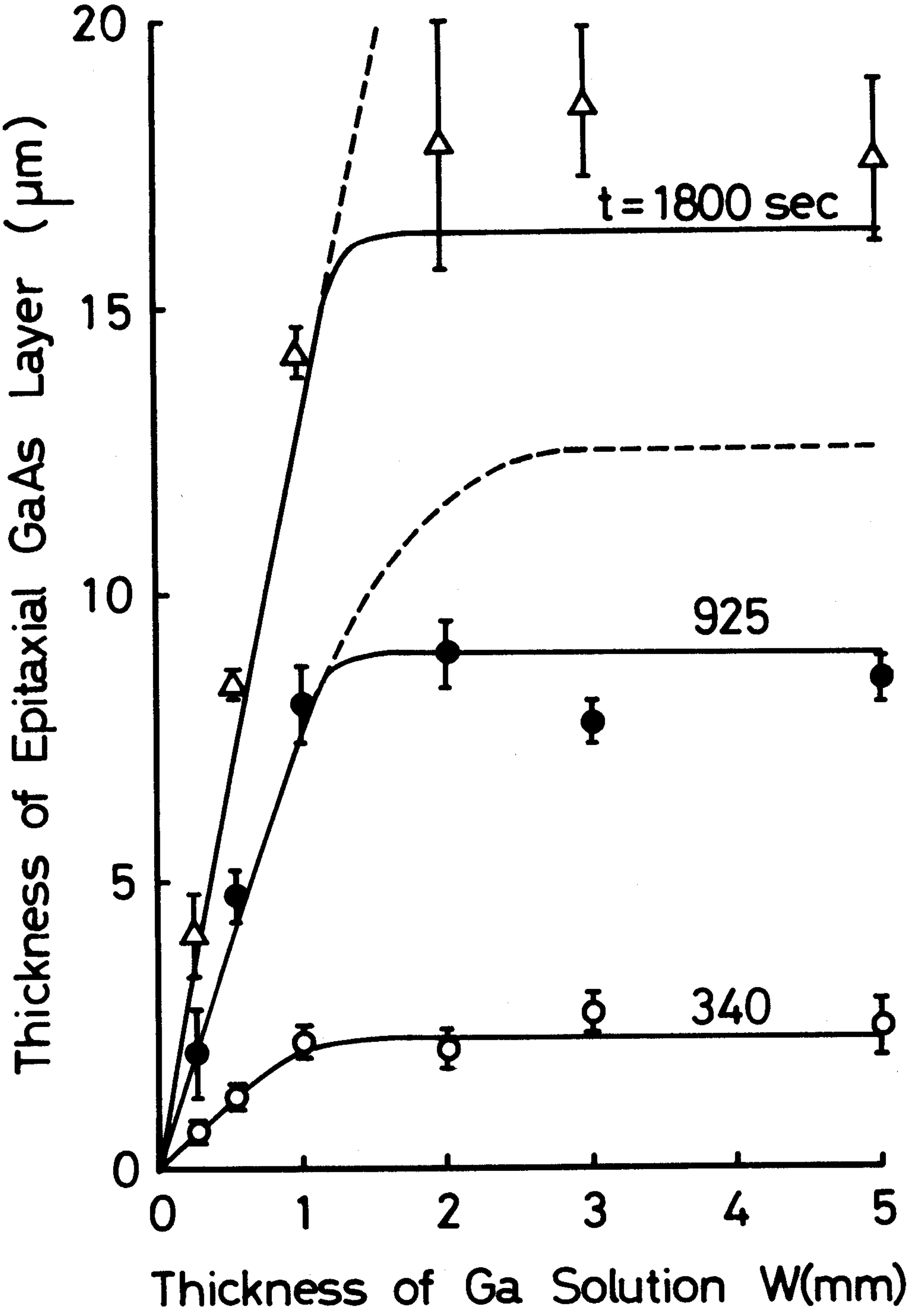

Fig. 4. Thickness of LPE GaAs layer versus thickness of Ga solution for growth durations t of 340, 925, and 1800 sec.

detail in Section 3.2.6. When there is homogeneous nucleation in a part of the Ga solution, that part of the solution does not contribute to the growth of the epitaxial layer, but only to the formation of small crystallites. Thus the solid lines become constant and separated from the broken ones.

When the growth duration is 340 sec, the solid and broken lines coincide for every thickness of the Ga solution. This is because the growth duration is too short for the effects of homogeneous nucleation to appear clearly. Even in this case, when the thickness of the Ga solution is more than 1.3 mm, the thickness of the epitaxial layer is independent of that of the solution. This can be understood if it is assumed that the diffusion length of As in the solution is 1.3 mm, because the part of the Ga solution farther from the interface than the diffusion length does not contribute to the epitaxy.

When the solution is less than 1.2 mm thick, the thickness of the epitaxial layer is proportional to that of the solution. The solid lines also coincide with the calculated values obtained using Eq. (29). This means that almost all of the As atoms in excess of the equilibrium As concentration deposit onto the substrate.

Therefore, when the thickness of the solution is less than about 1 mm, fine control of a thin and uniform epitaxial layer can be realized because the thickness of the epitaxial layer decreases as that of the solution decreases and small crystallite formation which may lead to nonuniform epitaxial layer is suppressed.

3.2.2. The effect of the cooling rate

The dependence of the epitaxial layer thickness on the cooling rate for various thicknesses of the Ga solution is shown in Fig. 5. The solid and broken lines are calculated by the numerical method and by Eq. (30). An initial growth temperature of 744 °C, an initial supercooling of 0 °C, and a cooling range of 744-734.4 °C were assumed in the calculation.

In Fig. 5, the epitaxial layer thickness is dependent on the cooling rate when the thickness of the solution is more than 1 mm, while it is roughly constant when the thickness of the solution is less than about 0.5 mm.

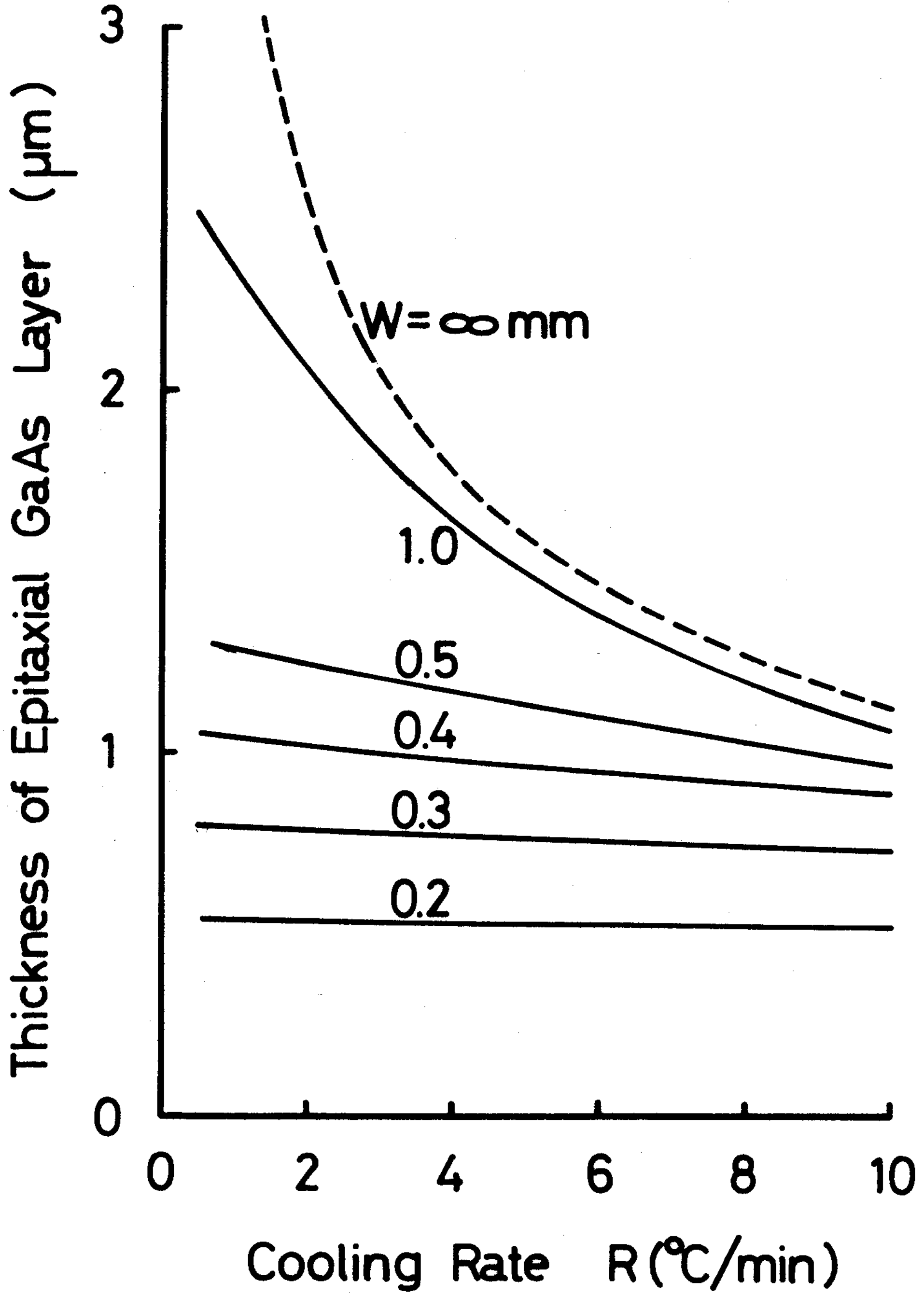

Fig. 5. Thickness of epitaxial GaAs layer versus cooling rate for various thickness W of Ga solution.

Therefore, if the Ga solution is chosen to be less than 0.5 mm thick, reproducible growth of thin epitaxial layers can be achieved by controlling the cooling range precisely.

3.2.3. The effect of initial supercooling

The dependence of the additional epitaxial layer thickness on the initial supercooling calculated by Eqs. (28) and (30) is shown for different thicknesses of the Ga solution in Fig. 6. An initial growth temperature of 744 °C, a cooling rate of 0 °C/min, and a growth duration of 4 min were assumed in the calculation.

As will be described later, some amount of initial supercooling is necessary for growing GaAs with a smooth surface. However, initial supercooling is not desirable for the growth of thin GaAs layers because it adds an excess growth layer to the normal layer as shown in Fig. 6. From Fig. 6, it is seen that a thinner Ga solution is desirable in order to obtain a thin GaAs epitaxial layer with a smooth surface.

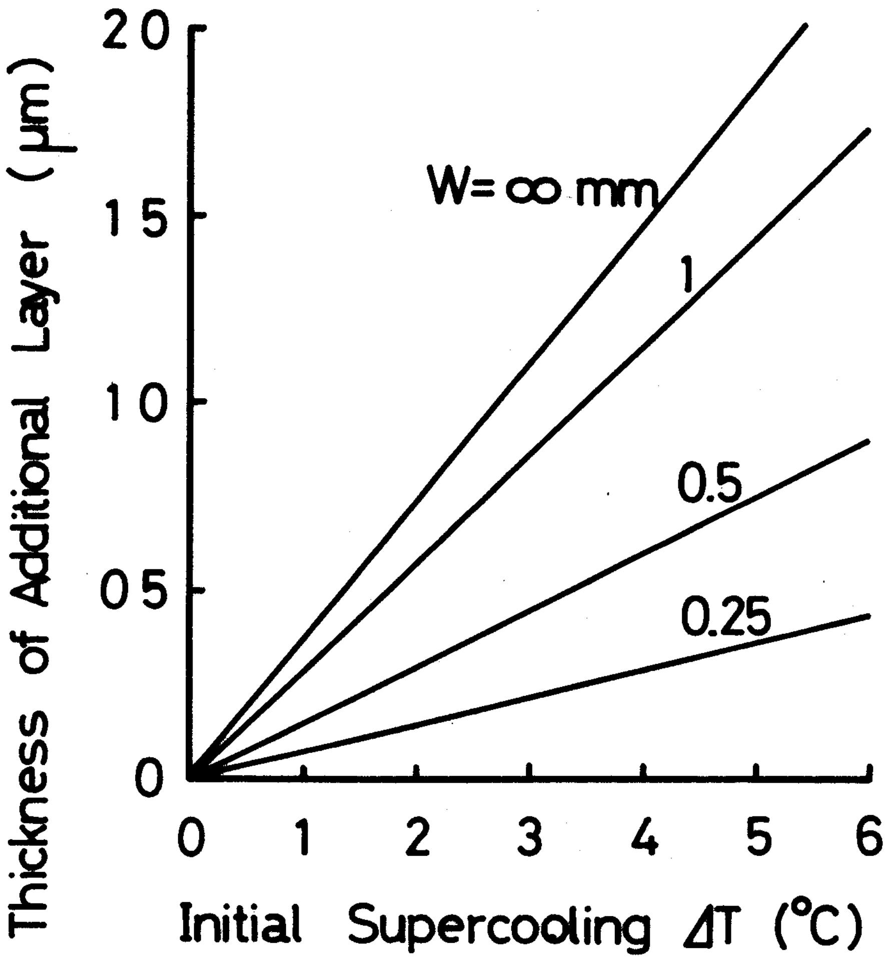

Fig. 6. Thickness of the additional epitaxial layer versus initial supercooling for different solution thicknesses W.

3.2.4. Influence of initial growth temperature

The dependence of the epitaxial layer thickness on the inital growth temperature calculated by Eq. (28) is shown in Fig. 7. A growth duration of 4 min, a cooling rate of 2.4 °C/min, and an initial supercooling of 0 °C were assumed in the calculation.

It can be seen from Fig. 7 that the thickness of the epitaxial layer depends on the initial growth temperature. Therefore, decreasing the initial growth temperature is also very effective for growing thin GaAs layers. For example, the thickness of the epitaxial layer decreases by about 43 % when the initial growth temperature is decreased from 750 to 700 °C.

3.2.5. Influence of growth duration

The relationship between the thickness of the epitaxial layer and the growth duration is shown in Fig. 8. The solid lines are the plots of the theoretical values for two different initial supercoolings. The deviations of the experimental

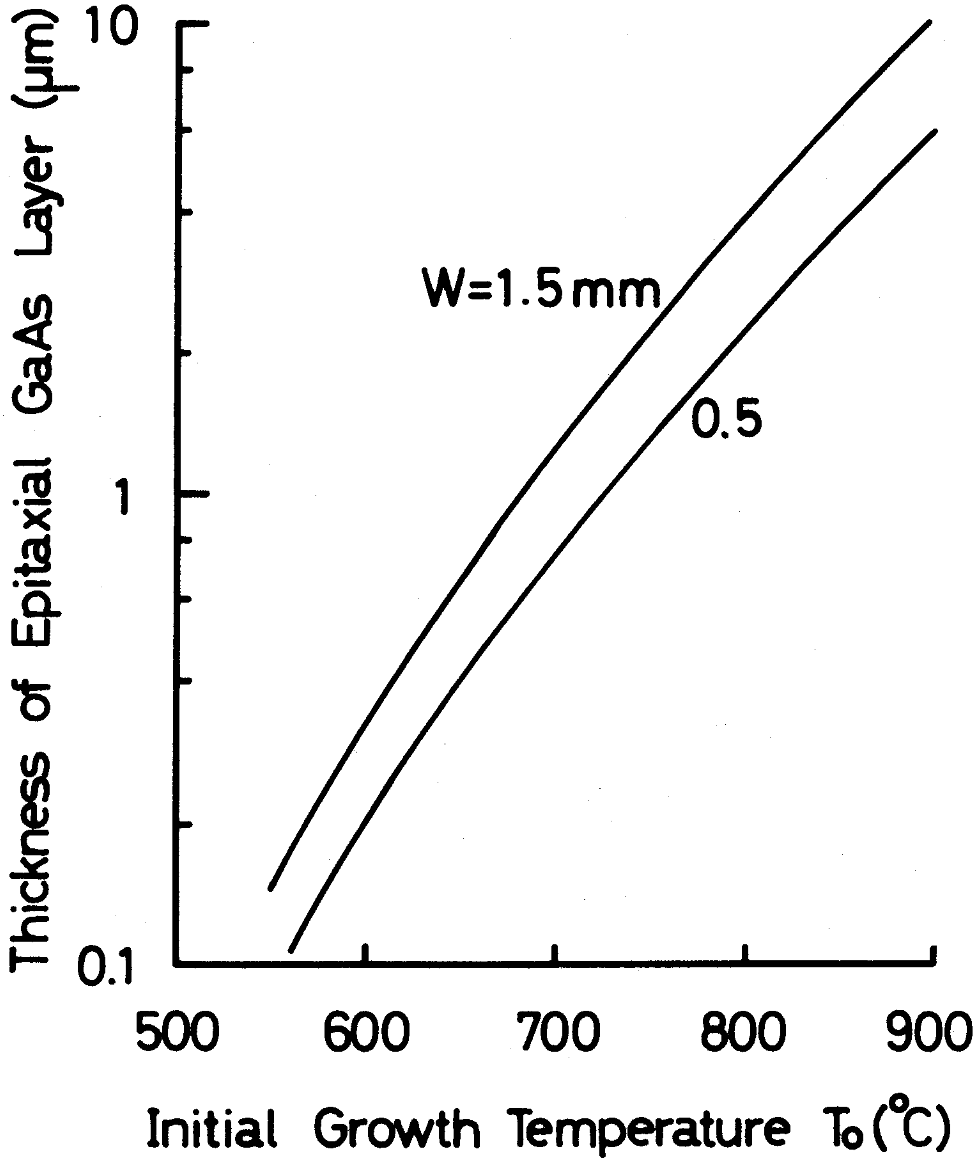

Fig. 7. Thickness of epitaxial GaAs layer versus initial growth temperature for two solution thickness W.

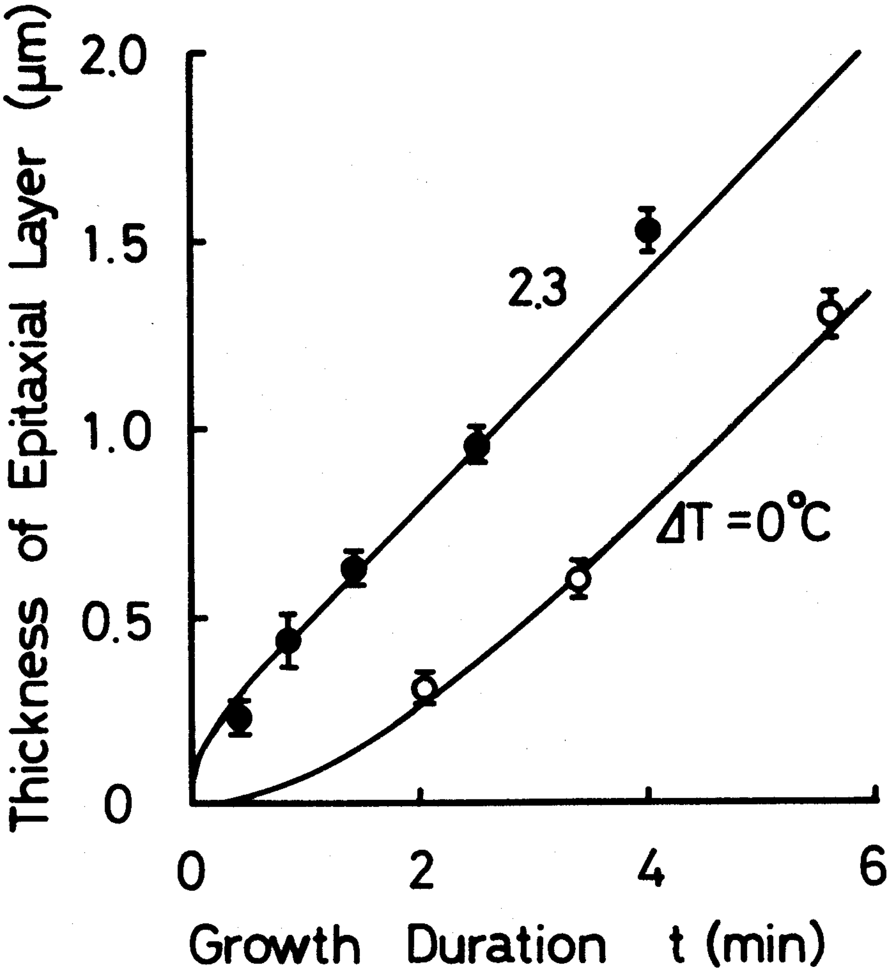

Fig. 8. Thickness of epitaxial GaAs layer versus growth duration.

values show the lateral variation of the layer thickness. Calculations were carried out under the assumption that the growth temperature is 744 °C, the cooling rate 2.4 °C/min, and the thickness of the Ga solution 0.5 mm. The theoretical values were obtained by taking into account the transient variation of the cooling rate during the initial stage of cooling.

It can be seen from Fig. 8 that the thickness of the epitaxial layer is proportional to the growth duration, except during the first minute. In the experiment, the surface of the epitaxial layer was flat and smooth when the layer was grown using a Ga solution supercooled by 2.3 °C, whereas the surface was wavy when the layer was grown using a saturated solution. Therefore, some degree of supercooling is necessary for obtaining smooth surface, as has been reported elsewhere35).

3.2.6. The experimental evidences for critical supercooling and the diffusion coefficient of As in Ga solution

Hsieh⁷⁾ has recently reported that an initial supercooling of 5 °C was insufficient for spontaneous nucleation. Moreover, Crossley and Small²⁴⁾ have reported that the critical supercooling was 15-20 °C. However, the exact value of critical supercooling has not been determined.

The dependence of the epitaxial layer thickness on the initial supercooling is shown in Fig. 9. In this figure, the experimental results (solid circles) are compared with the calculated values (solid lines) for different critical supercoolings. Epitaxial layers of GaAs were grown between 744 and 739 °C from Ga solutions which were initially supercooled by 0 to 30 °C. The thickness of the Ga solution was 0.5 mm and the cooling rate 2.4 °C/min.

As seen from Fig. 9, the calculated values agree with the experimental ones if it is assumed that the critical supercooling is 6 °C.

The As concentration profile in the Ga solution calculated using the same growth parameters used in

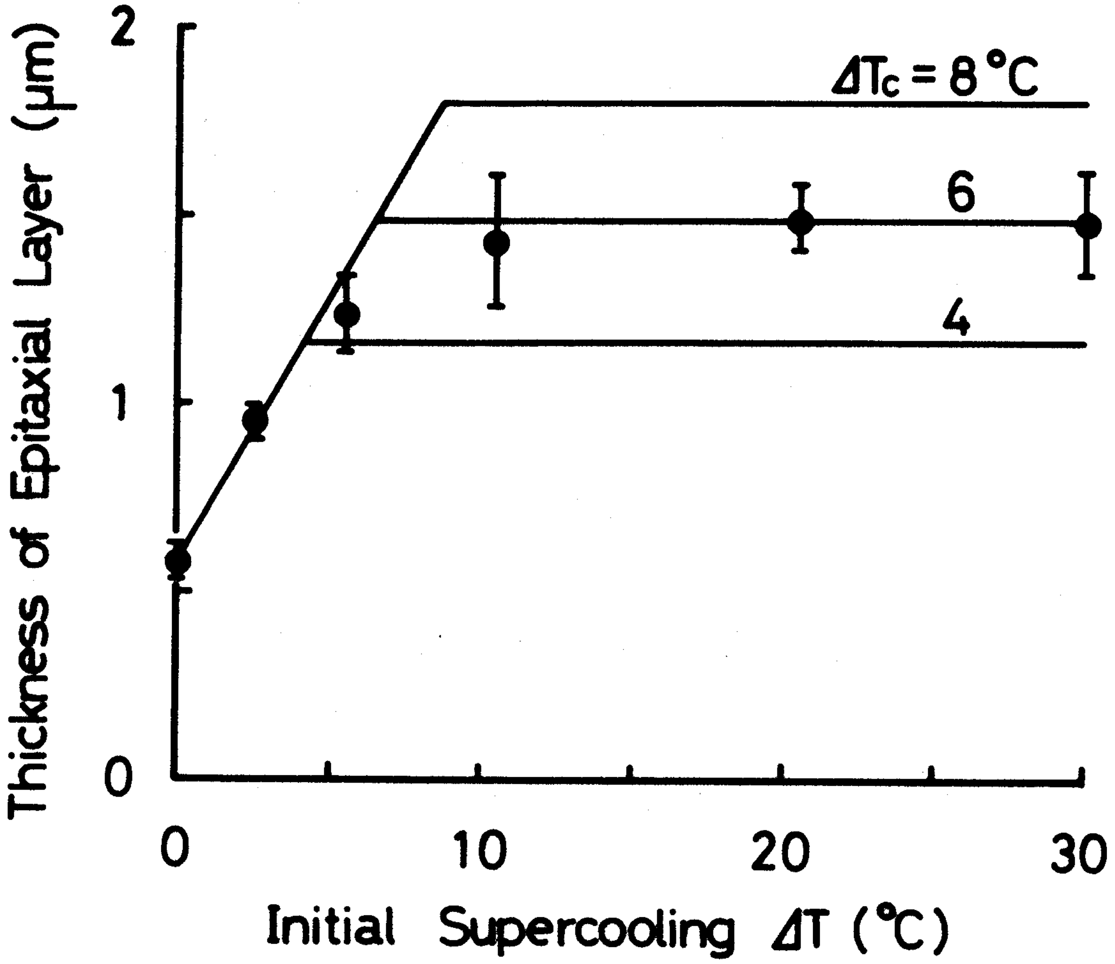

Fig. 9. Thickness of epitaxial GaAs layer versus initial supercooling. Solid lines show the calculated values for different critical supercooling.

Fig. 4 is shown in Fig. 10. The solid and broken lines show the calculated results for $\Delta T_c = 6\,^\circ C$ and $\Delta T_c = \infty\,^\circ C$, respectively.

When the thickness of the solution is 0.5 or 1 mm, the solid and broken lines coincide with each other. However, when the thickness of the solution is 1.5 mm, the solid and broken lines are separated. Moreover, the solid line become parallel to the abscissa when the distance from solid-liquid interface is more than 1.2 mm. That is, homogeneous nucleation starts about 1.2 mm from the solid-liquid interface. Therefore, it can be concluded that the effect of homogeneous nucleation can be neglected when the thickness of the solution is less than 1.2 mm. This result coincides well with an experimental result shown in Section 3.2.1. The critical distance x_c, where the homogeneous nucleation occurs, depends on the cooling rate. Therefore, the selection of an appropriate pair of cooling rate and solution thickness is very important for keeping the solution free from small crystallites.

The relationship between the thickness of the GaAs epitaxial layer and the growth duration is shown in Fig. 11. The solid lines are the calculated

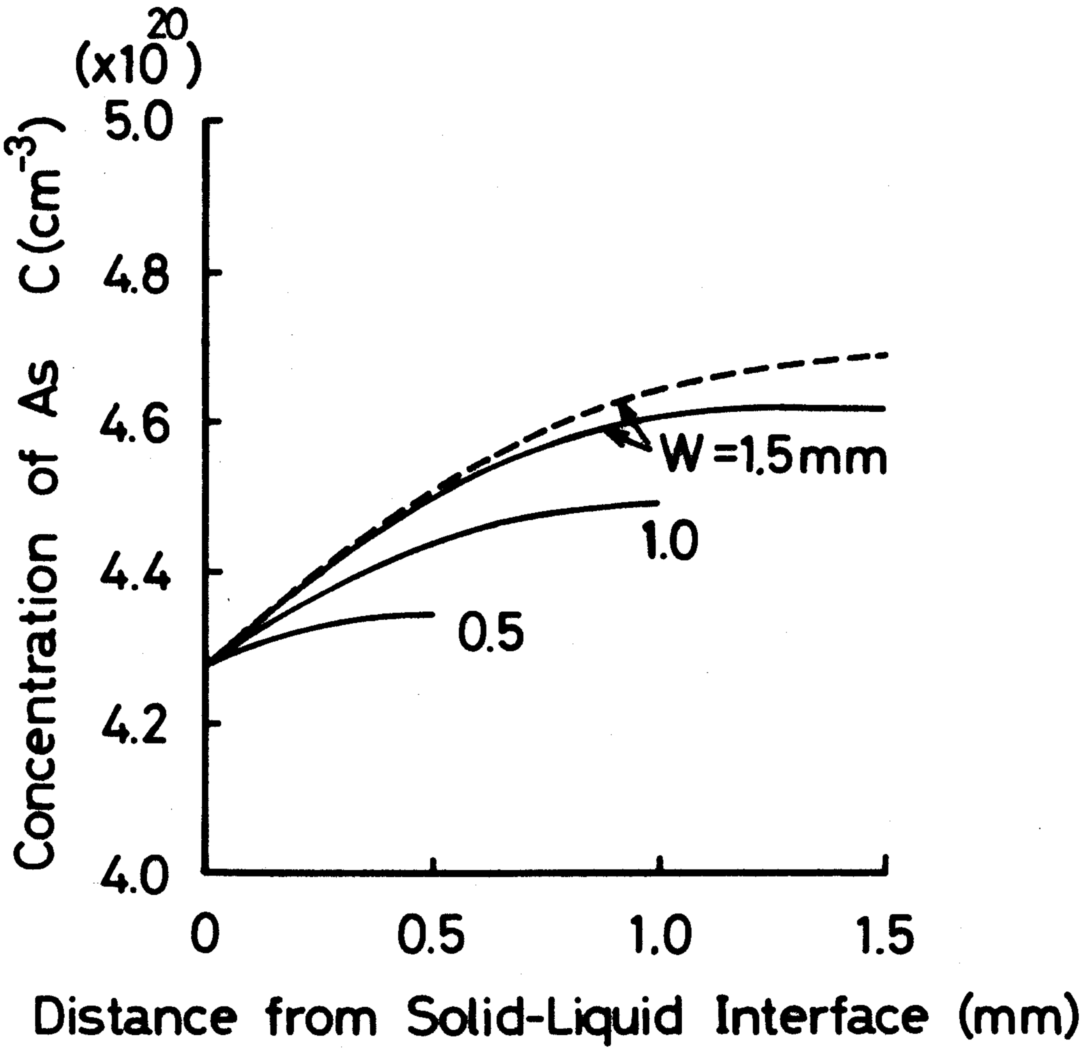

Fig. 10. As concentration profile in Ga solution at 731 ℃ for different solution thicknesses W.

values for different diffusion coefficients and the solid circles are the experimental values. The growth parameters used are as follows : initial growth temperature, 744 °C; initial supercooling, 0 °C; and solution thickness, 10 mm.

In order to obtain the diffusion coefficient of As, the solution thickness was chosen to be thicker than the diffusion length of As, $(Dt)^{1/2}$. Moreover, in order to minimize the effect of homogeneous nucleation, a maximum growth duration of 6 min, roughly equal to the 340 sec of the case discussed in Section 3.2.1, was chosen. The calculated values include the correction for the transient variation of the cooling rate as $a'=a\ 1-\exp(-at/\delta)$, where a' is the corrected cooling rate, a=2.4 °C/min, and $\delta=4$ °C.

It is seen in Fig. 11 that the experimental values agree well with the calculated ones when the diffusion coefficient of As in Ga solution is 5×10^{-5} cm^2/sec at 744 °C.

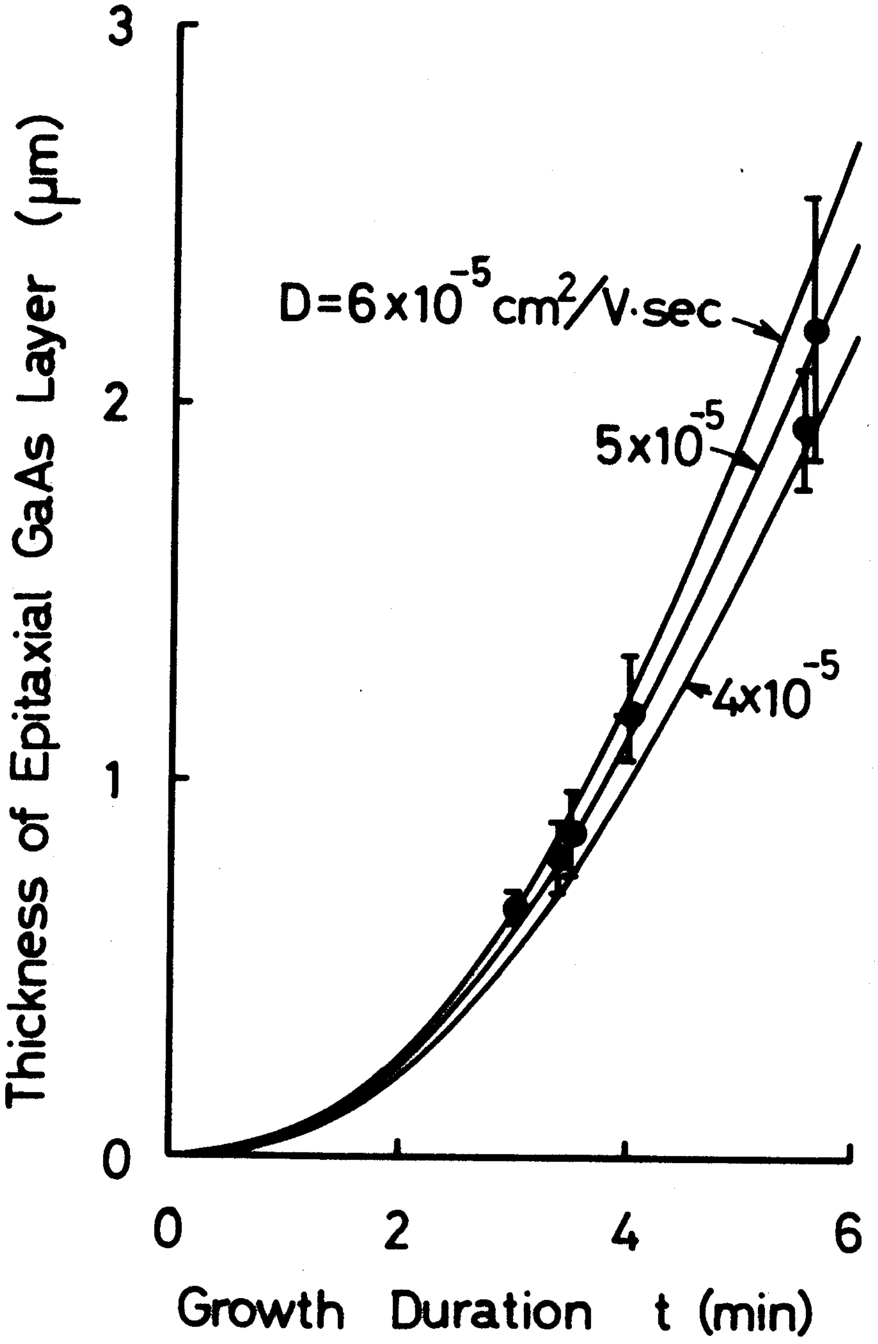

Fig. 11. Comparison between the experimental values of GaAs layer thickness and the calculated results for different diffusion coefficients D.

3.3. Growth Apparatus and Procedure for Multiple Layer Growth

The GaAs multiple layers were grown in a horizontal sliding boat made of high purity graphite. A cross sectional view of the boat is shown in Fig. 12. The important feature of this boat are the confinement of the Ga solution and the introduction of a dummy crystal. In this new LPE technique, the dummy crystal is placed in contact with a supercooled Ga solution before growth. The resulting As distribution in the Ga solution is shown schematically in Fig.13(a). Then the solution is brought into contact with the substrate when the As diffusion length becomes larger than the solution thickness, i.e. when $t \gg W^2/D$, where W is the solution thickness and D the diffusion coefficient of As in Ga solution. The resulting As concentration plofile is shown in Fig. 13(b). It is seen from Fig. 13 that the local supercooling at the bottom of the Ga solution can be controlled by the dummy crystal.

A GaAs (100)-oriented semi-insulating substrate was mechanically polished and subsequently chemically etched in a 4:1:1 solution of H_2SO_4:H_2O_2:H_2O .

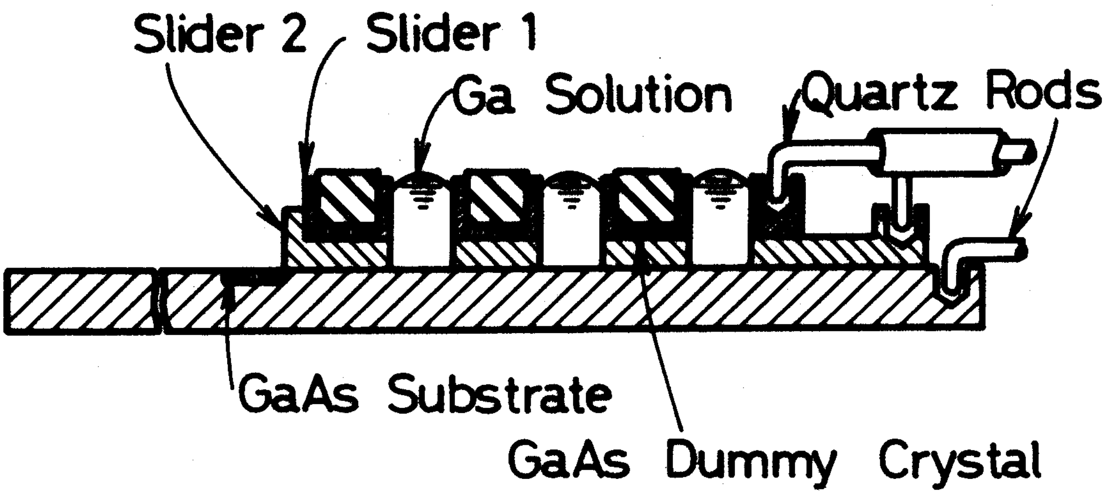

Fig. 12. Cross sectional view of the newly developed horizontal sliding boat.

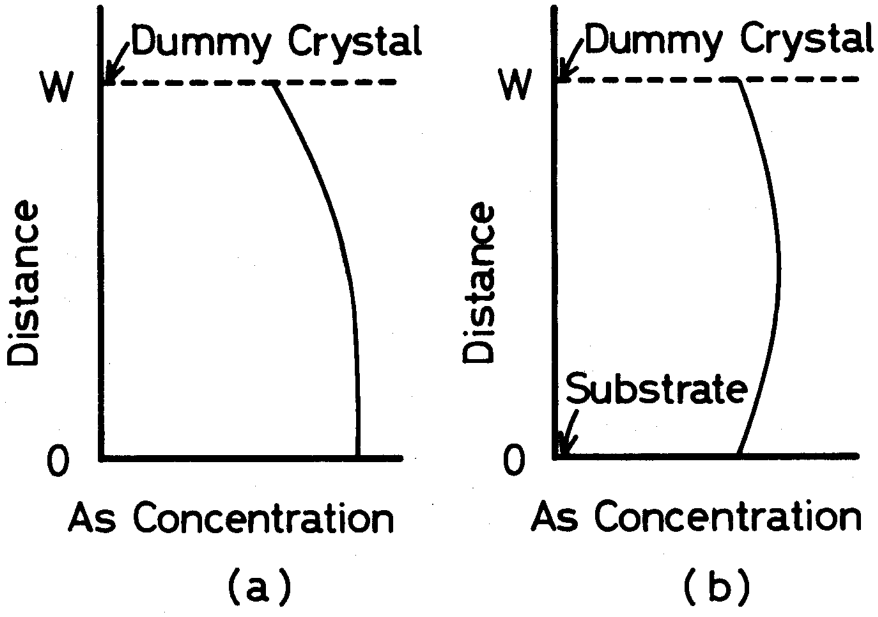

Fig. 13. As distribution in Ga solutions. (a) Only the dummy crystal is contacted by the solution. (b) Both the dummy and substrate crystal are contacted by the solution.

The substrate and solutions were loaded in the boat and placed in a uniform temperature zone (± 0.5 °C). After purging with hydrogen, the boat was maintained at a temperature of 750 °C for more than four hours. During this step, the solution was saturated with the source material and volatile impurities were removed.

Subsequently, the boat was cooled at a constant rate of 0.46 °C/min and the dummy crystals were slid over the Ga solution by pulling slider 1 (Fig. 12). The distance between the dummy and the substrate was 2 mm. Simultaneously, the excess GaAs source material floating on the surface of the solution was removed. Then epitaxial growth of the first layer was started at 749 °C by pushing sliders 1 and 2 at the same time. After a specified time period, the same process was repeated for the growth of each successive layer until the process was completed. Then the Ga solution was wiped off and epitaxial growth stopped.

The epitaxial wafer was then cleaved and stained to show the interface between the layers. The thickness of the thick epitaxial layers was measured using an optical microscope. The thickness of the thin layers was determined from the carrier concentration profile, which was obtained by a conventional differential capacitance technique[46].

3.4. Results and Discussion for Multiple-Layer Grpwth

3.4.1. Control of local supercooling

The time dependence of local supercooling at the bottom of the Ga solution (ΔT_b) is shown in Fig. 14. Growth time is represented by the corresponding cooling range. The dummy crystal is touched to the Ga solution at the saturation temperature (744 °C) and cooled at a constant cooling rate of 0.2 °C/min. But the substrate is still not touching the solution.

As cooling proceeds, the local supercooling of the thick solution increases by the same degree as the cooling range. But the local supercooling becomes saturated for solution thicknesses 0.5 and 3 mm in Fig. 14. The turning point corresponds to a cooling time $t=W^2/D$. Therefore, local supercooling before contacting the substrate can be kept constant if the cooling time after contacting the dummy crystal is selected to be greater than W^2/D. This feature is

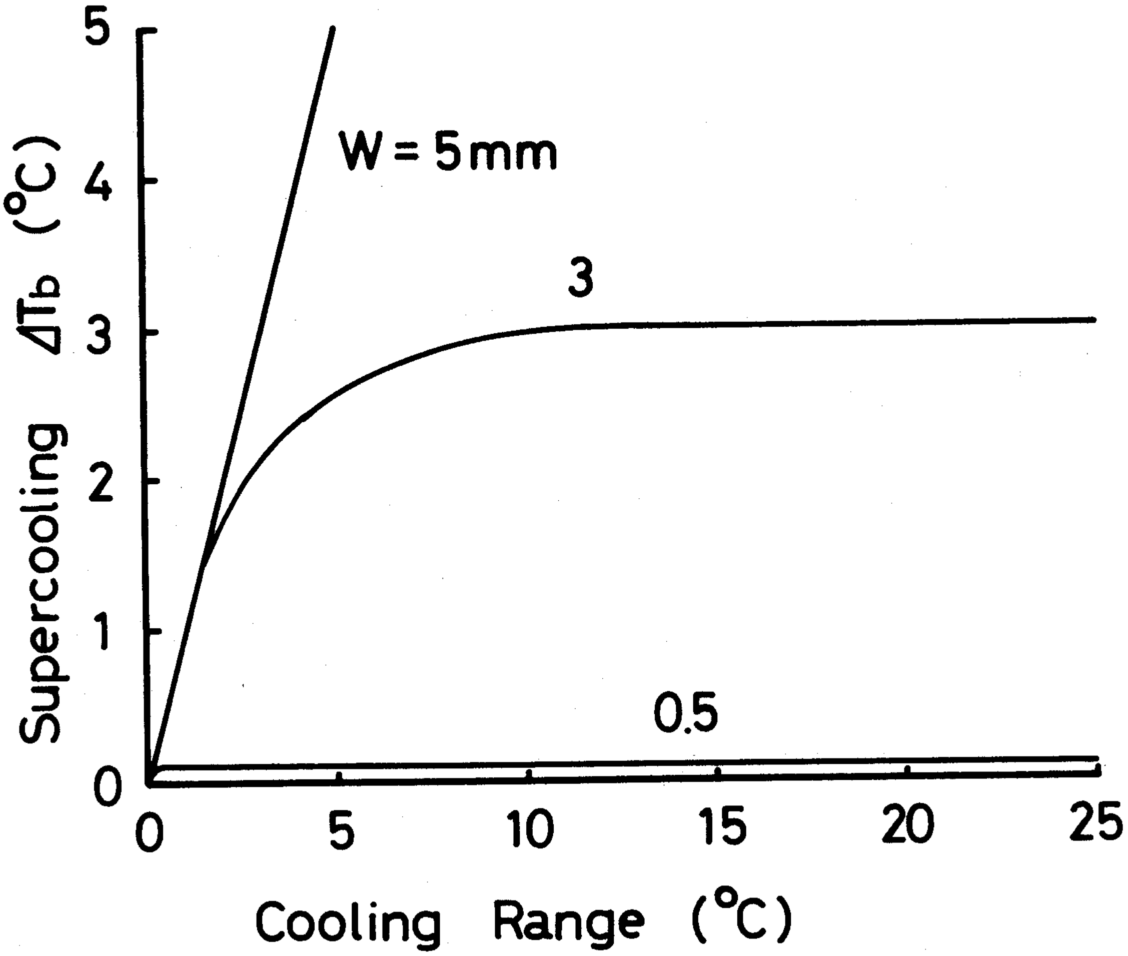

Fig. 14. Time dependence of local supercooling at the bottom of the solution. Growth time is represented by corresponding cooling range.

an advantage in the thickness control of the multiple layers grown by the successive growth.

The relationship between the saturated values of the local supercooling at the bottom of the solution (ΔT_b) and solution thickness was calculated at 744 °C for a cooling rate of 0.5-2.0 °C/min and is shown in Fig. 15. Growth conditions employed for the calculation are as follows : saturation temperature, 756 °C; contact temperature for dummy crystal, 750 °C. It is seen from this figure that the local supercooling ΔT_b is roughly proportional to the cooling rate and the second power of the solution thickness. Therefore, maximum supercooling in the solution, i.e. local supercooling at the bottom of the solution ΔT_b, can be kept constant against time at a desired value. It is important to select a cooling rate and solution thickness which satisfy the conditions whereby the product aW^2 is less than a critical value. This is necessary so that the maximum supercooling in the solution is kept less than the critical supercooling (6 °C) and the Ga solution is kept free from GaAs precipitates.

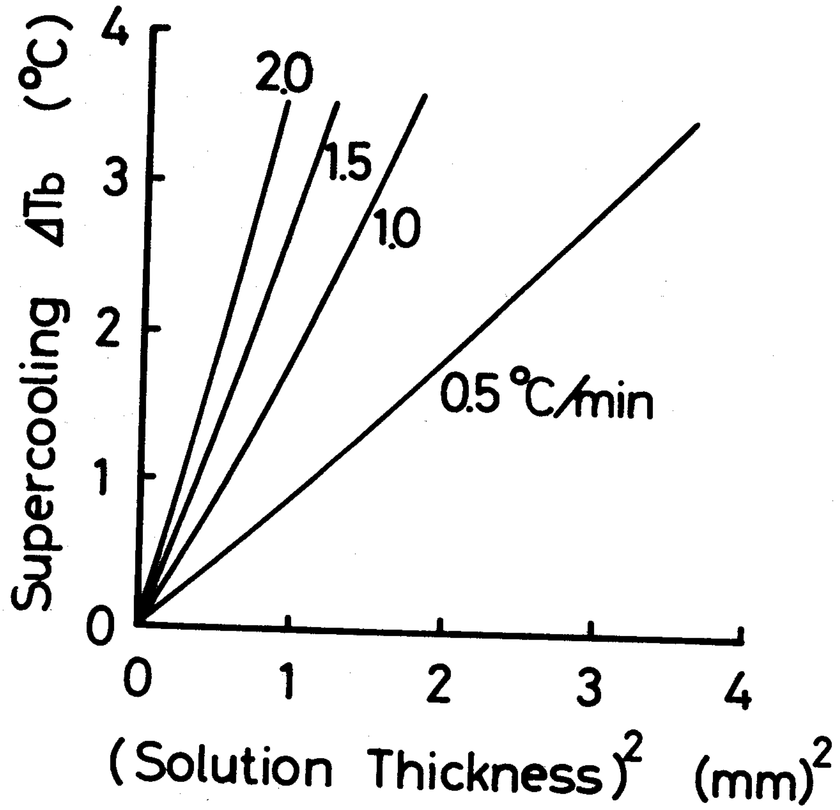

Fig. 15. Relationship between local supercooling at the bottom of the solution and the square of solution thickness at 744 °C for a cooling rate of 0.5-2.0 °C/min.

3.4.2. Layer thickness

The thickness of the first layer as a function of growth time is shown in Fig. 16. The curves are calculated results and the solid circles are experimental data. Curves (a), (b), and (c) correspond to the following three cases : (a) diffusion only with a dummy crystal, (b) boundary layer diffusion with a dummy crystal under solution stirring, and (c) diffusion only without dummy crystal ; the cooling range before touching the substrate is 1 °C for all cases. In the calculation of case (b), the existence of solution stirring is assumed and a diffusion boundary layer of 0.4 mm is used for both the dummy and the substrate crystals to get a good fit with experimental data. Cases (a) and (b) correspond to the present improved LPE and case (c) corresponds to the conventional one.

It can be seen from this figure that there is only a slight difference between curves (a) and (b). Moreover, the experimental results agree well with curves (a) and (b). When the solution thickness is smaller than the diffusion length of As, the epitaxial layer thickness is mainly limited by the maximum thickness which can be obtained from a finite

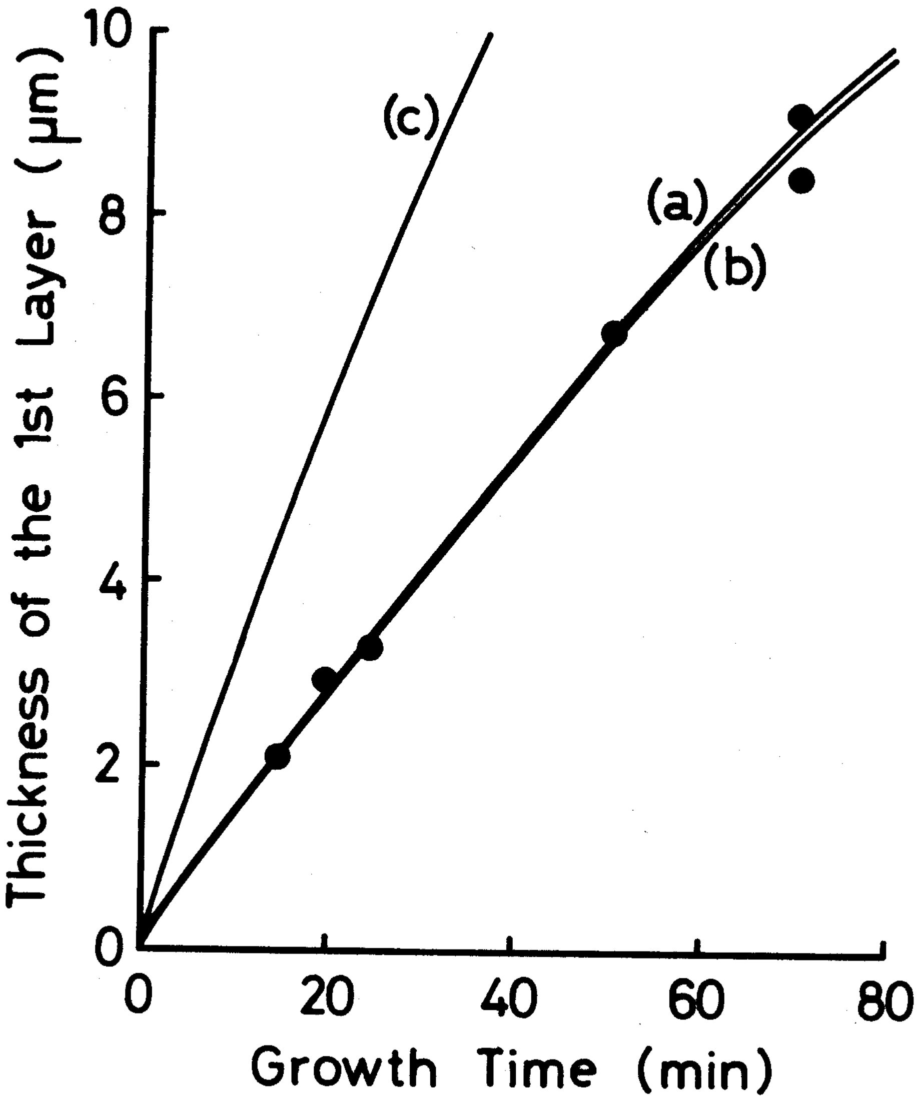

Fig. 16. Thickness of the first layer versus growth time. Solid circles are the experimental data and curves are the calculated results for cases (a) diffusion only with dummy crystal, (b) boundary layer diffusion with dummy crystal, and (c) diffusion only without dummy crystal.

solution[30]. As the cooling range is much larger than the initial supercooling in Fig. 16, the decrease in the local supercooling by stirring has only a slight effect on the layer thickness. By comparing curves (a) and (c), it is seen that the thickness of the epitaxial layer can be halved in the same growth time using this LPE method.

The thickness of the second layer as a function of growth time is shown in Fig. 17. The second layer was grown on the first layer (buffer layer for the GaAs FET's), which was about 9 μm in thickness. In this figure, the solid circles show the experimental results and the curves represent the calculated results for three cases : (a) diffusion only with a dummy crystal, (b) boundary layer diffusion with a dummy crystal, and (c) the conventional method, i.e. semi-infinite solution. As the second solution was cooled more than the critical supercooling, GaAs platelets should be present due to homogeneous nucleation when the solution thickness is semi-infinite. Accordingly, uniform supercooling of 6 ℃ is assumed for case (c).

In Fig. 17 there is a difference between curves (a) and (b) because the cooling range is not large

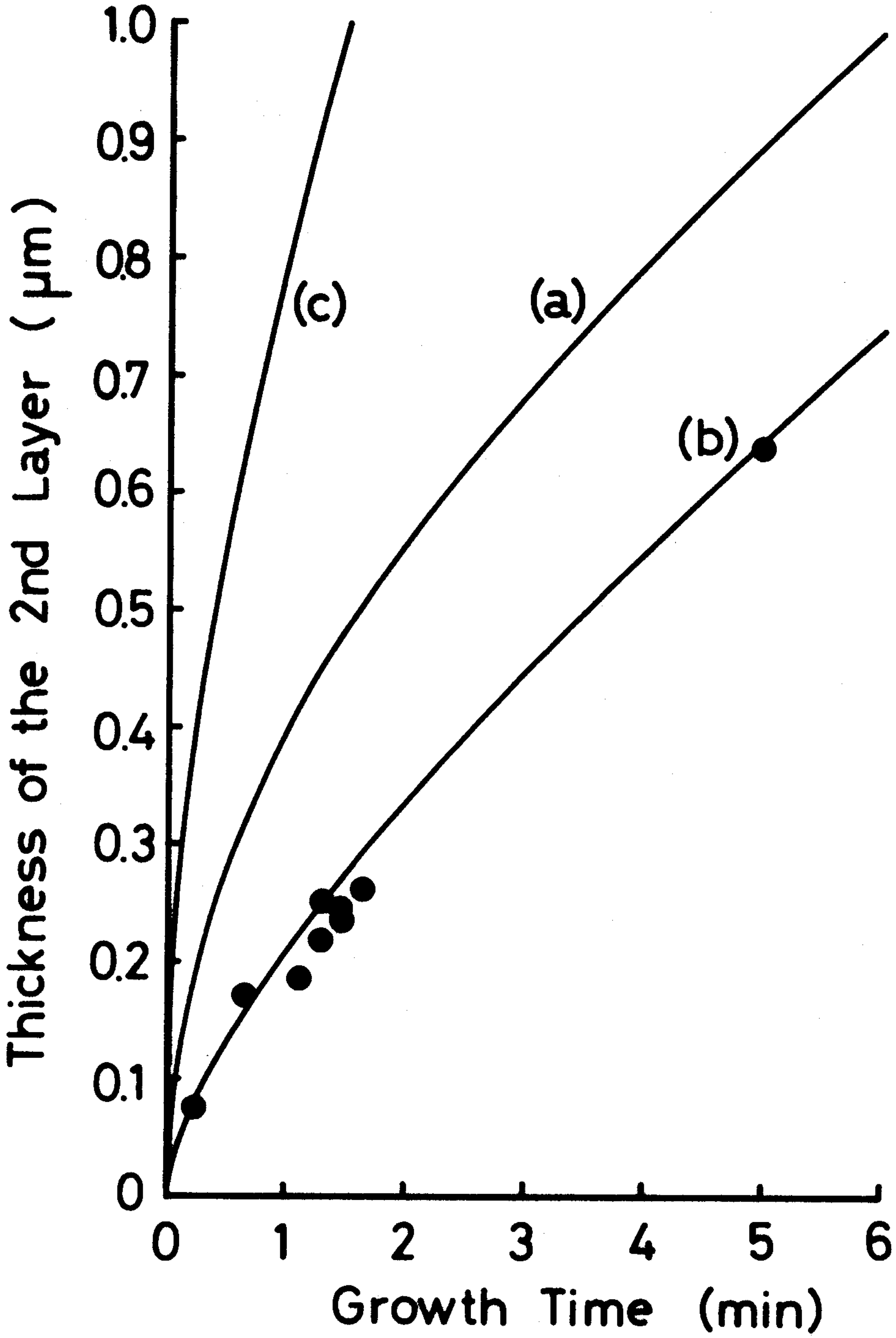

Fig. 17. Thickness of the second layer versus growth time. Solid circles are the experimental data and curves are the calculated results for cases (a) diffusion only with dummy crystal, (b) boundary layer diffusion with dummy crystal, and (c) the conventional method.

enough. It is also shown by Figs. 16 and 17 that the difference between curves (a) and (b) is roughly independent of time when $t > W^2/D$. In Fig. 17, the experimental results coincide well with curve (b), which was obtained assuming that the boundary layer thickness is 0.46 mm. This suggests the existence of stirring, which may be caused by the unstable density difference[24,34] in the solution.

The thickness dependence of the third layer on the growth time was almost the same as in Fig. 17. This is because the amount of cooling during the growth of the second layer was less than 2.5 °C. In addition, the local supercooling at the bottom of the solution was kept constant during the small temperature drop due to the existence of the dummy crystal.

4. LIQUID PHASE EPITAXY OF TERNARY Ga-Al-As

4.1. Phase Diagram

The analysis for the LPE of binary Ga-As system has been extended to the LPE of ternary Ga-Al-As system. The phase diagram of the ternary system is given by the following equations :

$$1-x = 4\ N_{Ga}N_{As}\frac{\gamma_{Ga}\ \gamma_{As}}{\gamma_{Ga}^{sl}\ \gamma_{As}^{sl}}$$

$$\exp\left\{ \Delta S_{GaAs}^{F}\ (T_{GaAs}^{F}-T)/R_0T \right\}, \qquad .....(33)$$

$$x = 4\ N_{Al}N_{As}\frac{\gamma_{Al}\ \gamma_{As}}{\gamma_{Al}^{sl}\ \gamma_{As}^{sl}}$$

$$\exp\left\{ \Delta S_{AlAs}^{F}\ (T_{AlAs}^{F}-T)/R_0T \right\}, \qquad .....(34)$$

under the restriction :

$$N_{Ga} + N_{Al} + N_{As} = 1\ , \qquad .....(35)$$

where γ and N are the activity coefficient and the mole fraction of the indicated element in the liquid, x the mole fraction of AlAs in the solid, ΔS^F the entropy of fusion for GaAs or AlAs, T the temperature, and R_0 the gas constant. The activity coefficients for a ternary liquid are given by the following equation and cyclic permutation of the indices,

$$R_0T \ln \gamma_{Ga} = \alpha_{GaAs} N_{As}^2 + \alpha_{GaAl} N_{Al}^2 + (\alpha_{GaAs} - \alpha_{AlAs} + \alpha_{GaAl}) N_{As} N_{Al} \, , \quad .....(36)$$

where α is the interaction parameter of the indicated system. Thermodynamic parameters used in the phase diagram calculation, which were obtained in the literature47,48), are listed in Table 1.

The equations (33) and (34) are so complicated that the isoaluminum curves of As mole fraction was approximated as below in order to reduce computer time :

$$N_{As} = K_1(N_{Al}) \exp(-A_1(N_{Al})/T), \qquad .....(37)$$

where

$$K_1(N_{Al}) = 4644 + 1.56\text{x}10^8 \, N_{Al}^{1.4} - 1.35\text{x}10^{12} \, N_{Al}^{3.6} \, ,$$

Table 1. Thermodynamic parameters used in the calculation of the Ga-Al-As phase diagram.

	Ga-As	Al-As	Ga-Al
Temperature of Fusion T^F (K)	1511	2043	—
Entropy of Fusion S^F (eu)	16.64	15.6	—
Interaction Parameter α (cal/mole)	$-9.16T+5160$	$-5.5T-6390$	104

$$A_1(N_{Al}) = \left[1.96 - 0.324\left\{\exp(-438.6\ N_{Al}) + \exp(-86.26\ N_{Al})\right\}\right] \times 10^4 .$$

In the region of 700-850 °C and $N_{Al} \leq 1$ %, this equation is a good fit to isoaluminum curves calculated using eqs.(33) and (34).

The temperature dependence of N_{As} was also calculated using Eqs (33) and (34), as shown in Fig. 18. The curves in this figure were again approximated in order to represent the $Ga_{1-x}Al_xAs$ layer thickness :

$$N_{As} = K_2(x)\ \exp(-A_2(x)/T), \qquad .....(38)$$

where

$$K_2(x) = K_0\ (1-x)\ \exp(\ 0.83x + 0.36x^2\ ),$$

$$K_0 = 4.64 \times 10^3,$$

$$A_2(x) = A_0\ (1 + 0.055x + 0.024x^2),$$

and

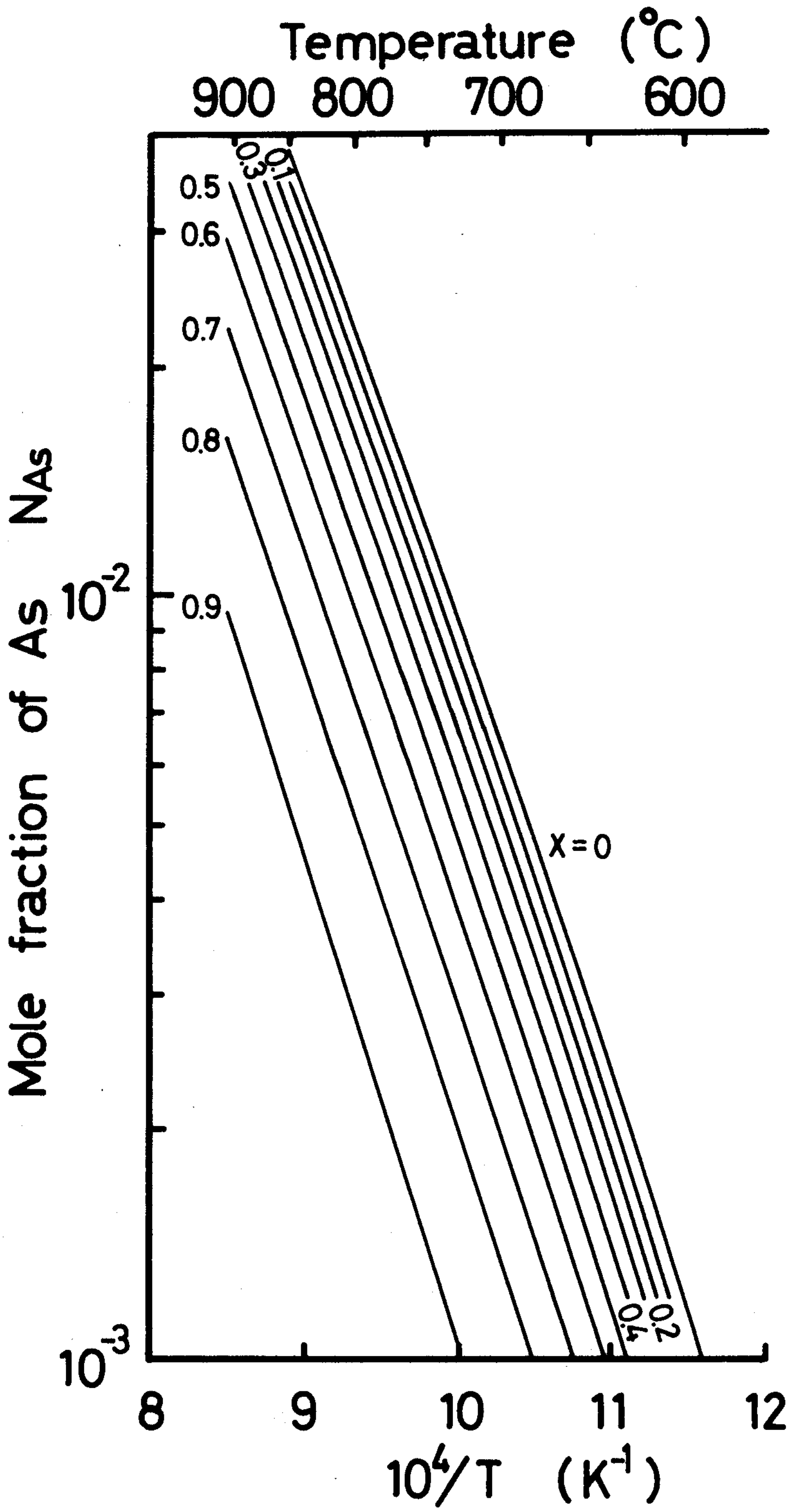

Fig. 18. Temperature dependence of As mole fraction in the saturated Ga solution.

$A_0 = 1.31 \times 10^4$ deg.

This equation gives a good fit to the curves in Fig. 18 in the region of 700-850 °C and $0 \leq x \leq 0.8$.

4.2. Boundary Conditions

A numerical method is applied to solve the one-dimensional diffusion equation taking into account the complicated boundary conditions which will be described later. The diffusion coefficient of Al and As in the Ga solution are both assumed to be equal to 5×10^{-5} cm^2/sec.

A simple initial condition of uniform liquid composition is assumed. At the solid-liquid interface, the following principal assumptions were made : (a) liquid and solid are in an isothermal condition and (b) the reaction kinetics are fast enough so that the liquid at the interface is in equilibrium composition. It is also assumed that there is no homogeneous nucleation in the solution.

A schematic phase diagram of the Ga-Al-As system and AlAs mole fraction in the solid are shown

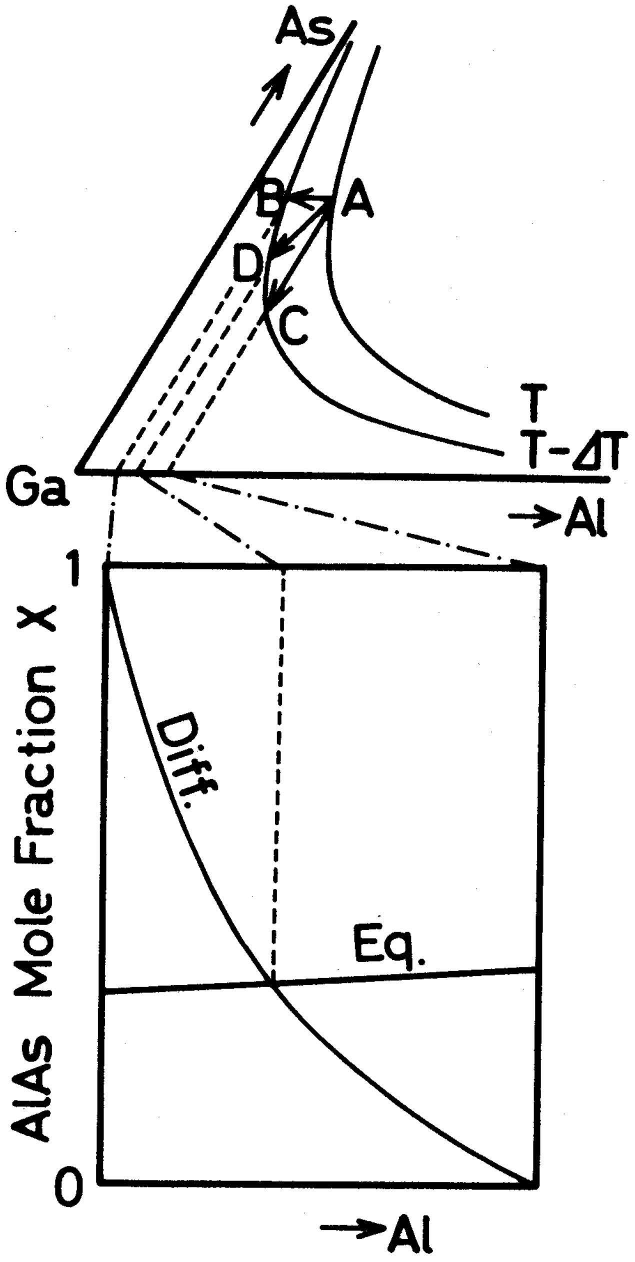

Fig. 19. The Ga-rich corner of the schematic Ga-Al-As ternary phase diagram and AlAs mole fraction.

in Fig. 19. The composition of the Ga solution saturated at temperature T is denoted as A in Fig. 19. When the temperature drops to T-ΔT' in a small time increment, local liquid composition at the interface varies to a point on the isotherm corresponding to the temperature of T-ΔT'. The equilibrium AlAs mole fraction on the isotherm BC is shown in Fig. 19. On the other hand, the AlAs mole fraction of the layer grown by cooling from A to a point on the isotherm BC can be calculated using the diffusion limited growth model and is also shown in Fig. 19.

It is clear from this figure that point D satisfies the boundary condition. Whenever the growth time is increased by a small time increment, the new local liquid composition at the solid-liquid interface is determined as mentioned above.

4.3. Convenient Approximation for the Layer Thickness

Now the crystal composition in the grown layer and the layer thickness can be calculated using the boundary conditions described in Section 4.2.

However, it is still meaningful to express the $Ga_{1-x}Al_xAs$ layer thickness as a function of the growth conditions in order to predict the layer thickness easily.

As will be shown in the following section, the variation of crystal composition in thin $Ga_{1-x}Al_xAs$ layers grown using a thick solution is less than about 10 %, so that it may be assumed that the crystal composition in the layer is constant. Then the temperature dependence of As saturation concentration can be approximated by the simple exponential dependence given by Eq. (38).

When x=0 the As saturation concentration is approximated by an exponential dependence which can be obtained by substituting x=0 into Eq. (38). Therefore, the epitaxial layer thickness of GaAs (L_{GaAs}) for a short growth time (t) and for a semi-infinite solution (solute diffusion length much less than solution thickness) is given by [30),]

$$L_{GaAs} = \left\{ 2A_0 \frac{\alpha_L K_0}{C_s} \left(\frac{D}{\pi}\right)^{1/2} \right\} \left\{ T_0^{-2} \exp(-A_0/T) \right\}$$

$$\left\{ \Delta T\ t^{1/2} + \frac{2}{3} a\ t^{3/2} \right\}, \qquad .....(39)$$

where T_0 the growth temperature, ΔT the initial supercooling, a the cooling rate, C_s the As concentration in solid, D the diffusion coefficient of As, and α_L the conversion factor ($\alpha_L = C_{As}/N_{As}$ where C_{As} is the As concentration in liquid). Therefore, epitaxial layer thickness of $Ga_{1-x}Al_xAs$ for a short growth time and for a semi-infinite solution can be obtained by substituting K(x) for K_0 and A(x) for A_0 in Eq. (39). Thus, the ratio of the epitaxial layer thickness L_{GaAlAs}/L_{GaAs} can be expressed as follows,

$$L_{GaAlAs}/L_{GaAs} = (1-x)\,(1 + 0.055x + 0.024x^2)\,\exp(\,0.83x + 0.36x^2\,)\,\exp(-1.31\times10^4(0.055x+0.024x^2)/T_0). \quad .....(40)$$

Equation (40) represents the dependence of the layer thickness on crystal composition x.

4.4. Crystal Composition

Variations of crystal composition with epitaxial layer thickness for cooling rates of 0.5 to 4.0 °C/min are shown in Fig. 20. The initial liquid composition used for the calculation is one typically used for the fabrication of double-heterostructure laser diodes. Initially, 3 mg of Al was dissolved in 4 g of Ga, then the solution was saturated at a temperature of 775 °C using a 2 mm thick solution.

The inhomogeneity of crystal composition can be improved by choosing a slow cooling rate. This is similar to the result obtained by Crossley and Small 49).

Variations of crystal composition with layer thickness for a solution thickness of 0.75 to 6.0 mm are shown in Fig. 21. The initial liquid composition is the same as the one used in Fig.20. The epitaxial growth was started at a saturation temperature of 775 °C using a slow cooling rate of 0.5 °C/min.

The magnitude of the variation in the crystal composition increases as the solution thickness decreases. The variations of crystal composition in the layers grown from 3 mm and 6 mm thick solutions

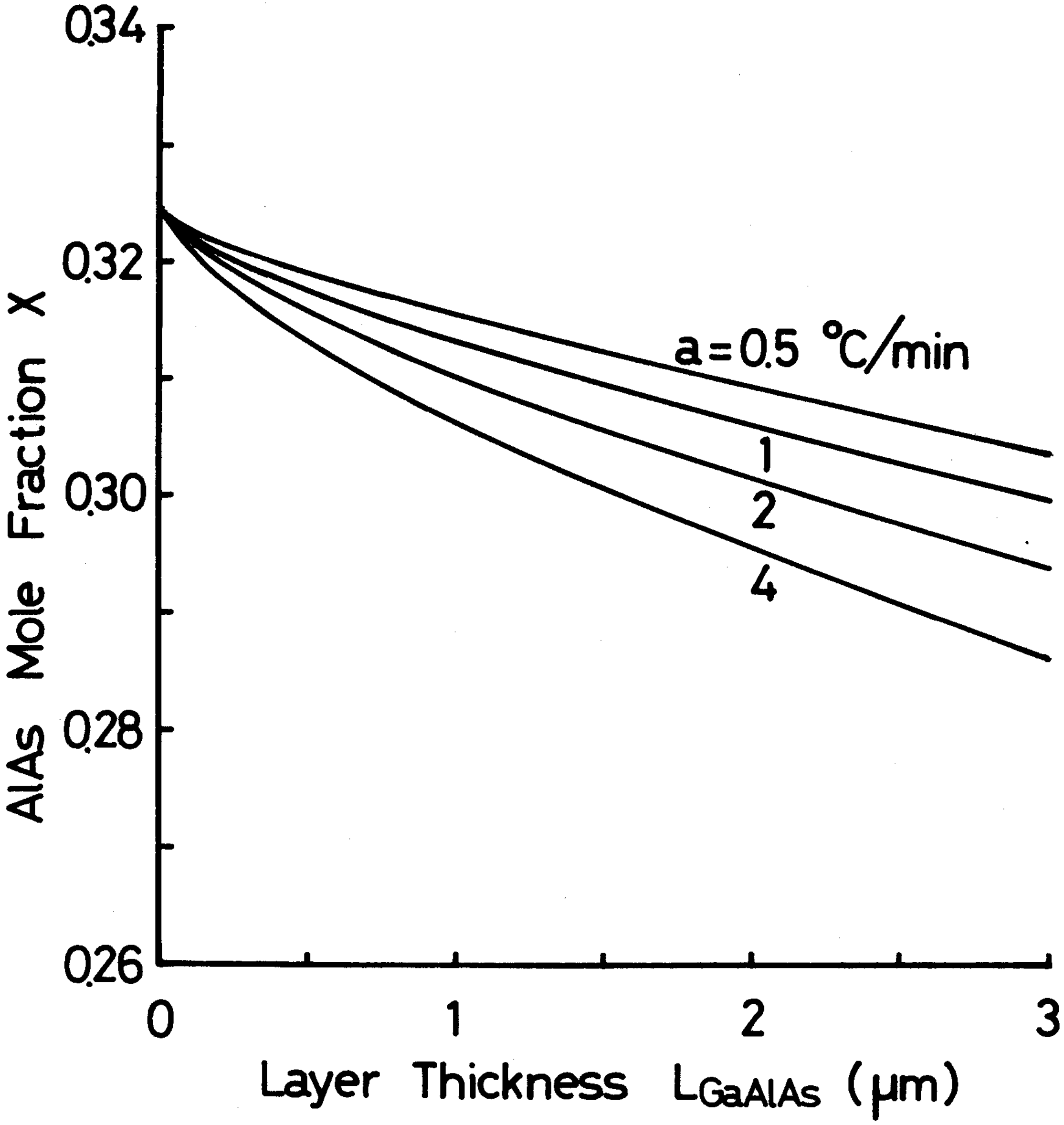

Fig. 20. Variations of the AlAs mole fraction in epitaxial layer with layer thickness for cooling rate of 0.5-4.0 °C/min.

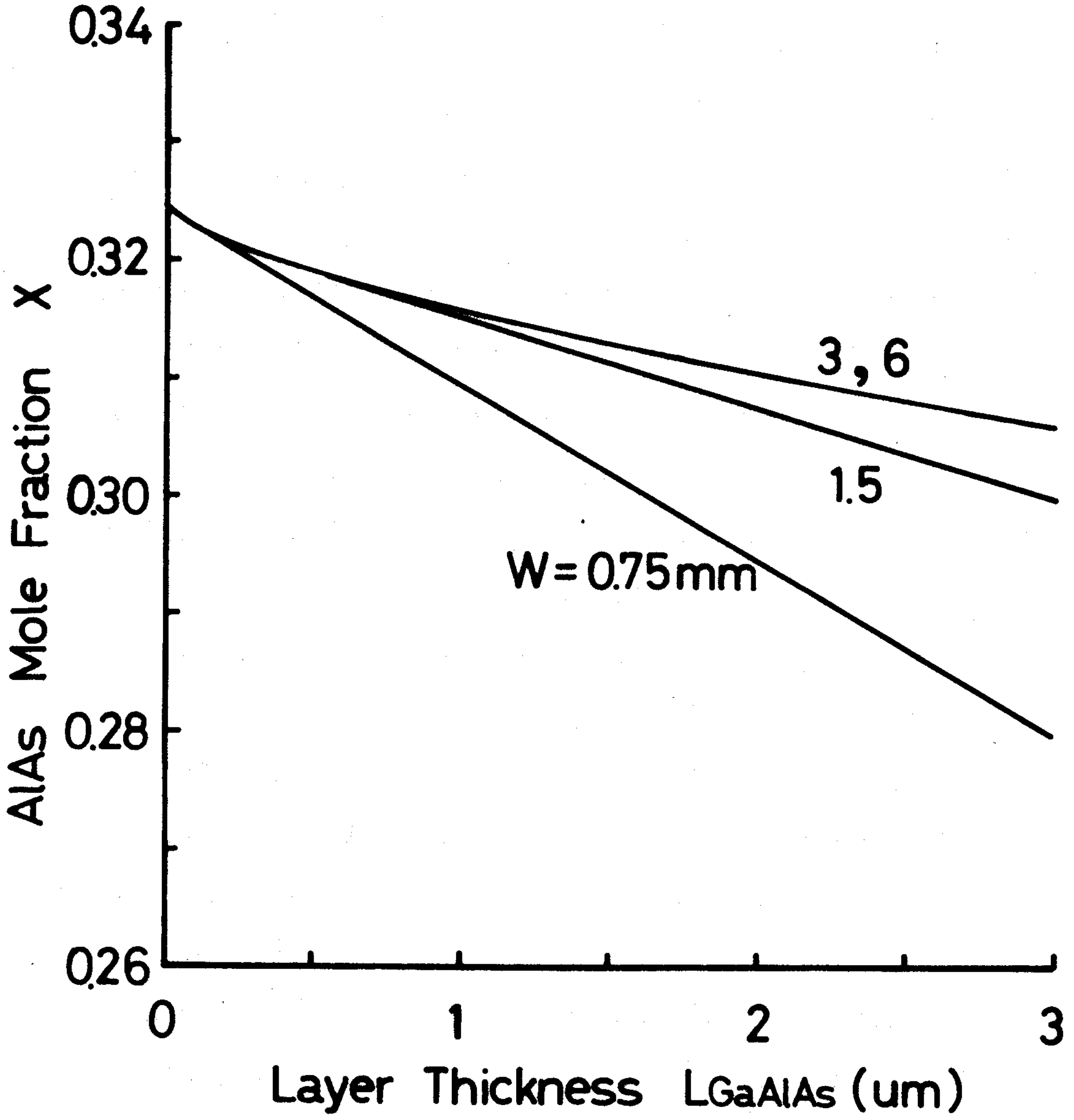

Fig. 21. Variations of the AlAs mole fraction in epitaxial layer with layer thickness for solution thickness of 0.75-6.0 mm.

are the same because the solution thickness is greater than the diffusion length of Al and As, i.e. these solution thicknesses can be regarded as semi-infinite. In the case of 0.75 mm and 1.5 mm thick solutions, the curves separate from that of the semi-infinite solution at a point where the diffusion length of the solute is roughly equal to the solution thickness. Consequently, a thin solution is not suitable for growing $Ga_{1-x}Al_xAs$ crystal with uniform AlAs composition along the layer thickness, although it is successfully applied for the growth of thin epitaxial layers27,30).

The variations of crystal composition with the layer thickness for initial supercooling of 0 to 6 °C is shown in Fig. 22. The amount of Al dissolved in the Ga solution is the same as that in Fig. 20. The epitaxial growth was started at 775 °C using a slow cooling rate of 0.2 °C/min and a solution of 2 mm thick. The solution was saturated at 0 to 6 °C above the growth temperature (775 °C) corresponding to the initial supercooling.

An epitaxial layer of $Ga_{1-x}Al_xAs$ with a uniform AlAs composition can be produced by increasing the the initial supercooling. This is because a small

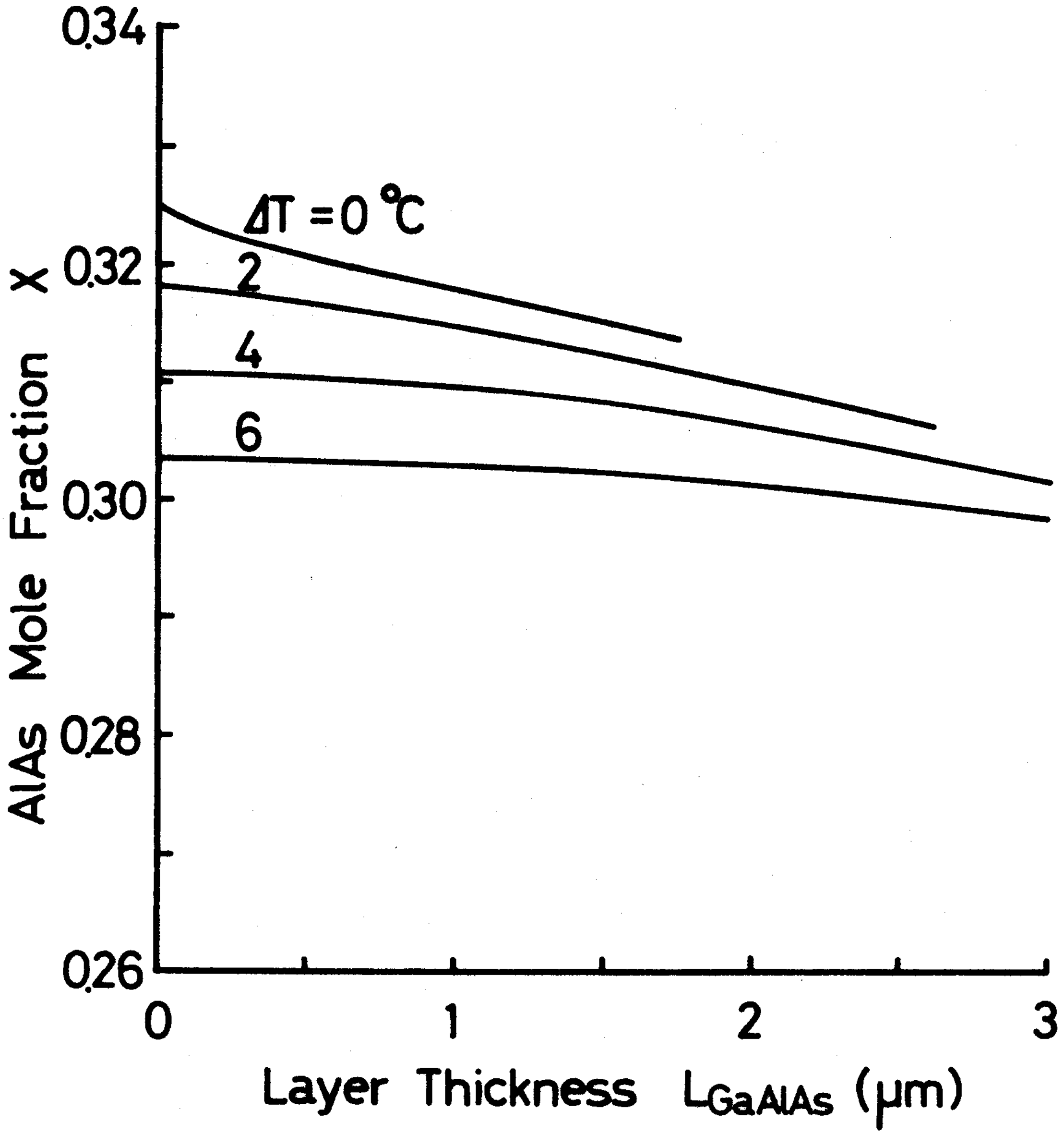

Fig. 22. Variation of the AlAs mole fraction in epitaxial layer with layer thickness for initial supercooling of 0 to 6 °C.

temperature drop is needed to obtain an epitaxial layer a few micrometers thick when the initial supercooling is increased.

The effect of the growth temperature on AlAs composition variations was examined. However, the variations of crystal composition around x=0.3 were almost the same as the ones at 775 °C in the temperature range of 700-850 °C.

4.5. Layer Thickness

The dependences of $Ga_{1-x}Al_xAs$ layer thickness on the growth temperature, the initial supercooling, the cooling rate, and the growth time were very similar to those of GaAs30) except for a factor which depends on the AlAs mole fraction. This is easily understood from Eqs (39) and (40).

In Fig. 23, curves (a) and (b) show the dependences of the layer thickness on crystal composotions calculated by numerical methods and by Eqs. (39) and (40), respectively. Experimental results are also shown in this figure. Growth conditions employed for the calculation

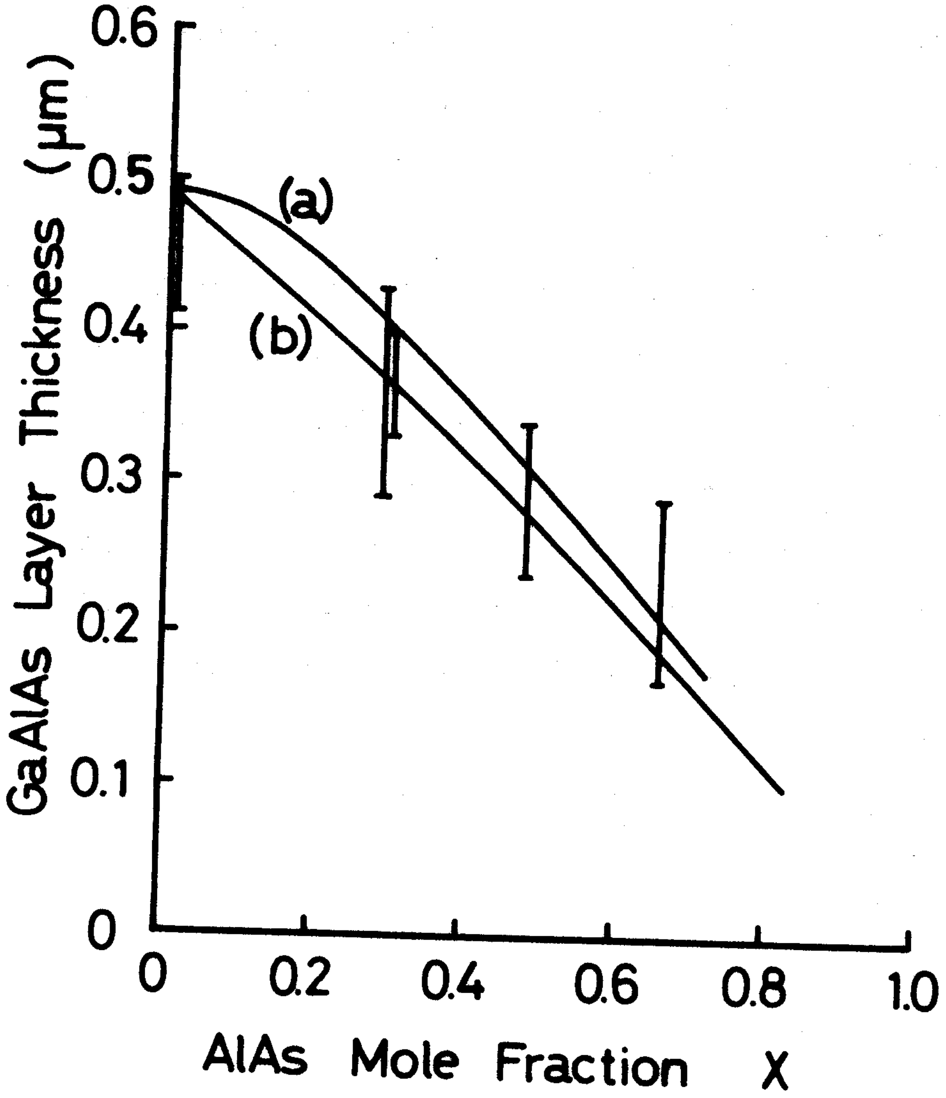

Fig. 23. Variation of $Ga_{1-x}Al_xAs$ layer thickness with AlAs mole fraction x.

and the experiment are as follows : initial supercooling, 1.2 °C; growth temperature, 699 °C; growth time, 210 sec; solution thickness, 5 mm; and cooling rate, 0.6 °C/min.

It is seen from this figure that the $Ga_{1-x}Al_xAs$ layer thickness decreases as x increases. Curves (a) and (b) in Fig. 23 are roughly proportional to (1-x). This means that the layer thickness is slightly influenced by the increase in the slope of the curves in Fig. 18 but is mainly influenced by the decrease in As solubility in the solution.

5. APPLICATIONS TO SOME DEVICES

5.1. GaAs TEO Diodes

5.1.1. Growth apparatus and procedure

Multiple layers of GaAs with an n^+-n-n^+ structure for TEO (Transferred Electron Oscillator) diodes were grown in a single operation. In the experiment, three kinds of Ga solutions were used : one was a lightly doped solution for a high purity active layer, which consisted of Ga (6-9's grade), undoped GaAs ($n=4\times10^{16}$ cm^{-3}), and a small fraction of tin ; the second was a heavily doped solution for a low resistance layer, which consisted of Ga and Se-doped GaAs ($n=1\times10^{18}$ cm^{-3}); and the third was a newly introduced purging solution of the same composition as the lightly doped solution for the active layer. The purging solution was put in the hole between the heavily doped solution and lightly doped solution.

The substrate crystal with (100)-orientation and doped with Te, Sn, Si, or Se to an electron concentration of about 10^{18} cm^{-3} was mechanically polished and chemically etched in a 4:1:1 solution of H_2SO_4:H_2O_2:H_2O.

After the substrate was loaded, the system was heated at 800 °C for more than 30 min. Then the system was cooled at a constant rate. The first n^+ buffer layer of a few micrometers was grown on the substrate by sliding the heavily doped solution onto the substrate Then the substrate was contacted with the purging solution and the solution remaining on the substrate was washed by the purging solution. By this washing process the carrier concentration change caused by the carry over of the Ga solution for n^+ buffer layer was minimized. Then an n-active layer and an n^+-contact layer were grown one after another. After the last n^+ layer was grown, the solution was removed and the system was cooled rapidly to room temperature.

5.1.2. Epitaxial layer doping profile

In this section, LPE of high purity GaAs and doping studies with Sn will be described. For the control of carrier concentration in the region of 10^{15}-10^{16} cm^{-3}, the residual impurities need to be lower than the desired carrier concentration. As small air leaks produce significant residual carrier concentrations, a leak-tight gas supply system was used. The dew point and the O_2 concentration in the H_2 gas were less than -70 °C and 0.04 ppm.

The growth temperature and preheat temperature have a large effect on the residual carrier concentration. The variation of residual carrier concentration as a function of growth temperature is shown in Fig. 24. The preheat temperature is 800 °C in this figure. The variation of the residual carrier concentration as a function of preheat temperature is shown in Fig. 25. In this figure, growth temperature is 20 °C lower than the preheat temperature. These figures show that major impurities can be removed by volatilization into the H_2 stream. Moreover, Fig. 24 shows that low growth temperature is required to minimize the residual impurities. The highest mobility obtained in this experiment was 9,000 $cm^2/V\cdot sec$ at room-temperature, and 130,000 $cm^2/V\cdot sec$ at 77 K. The electron concentration of the epitaxial layer was controlled in the region of 10^{15}-10^{16} cm^{-3} by the amount of Sn in the Ga solution. As the n layer was grown immediately after the growth of the n^+ buffer layer, the n layer was unavoidably doped by the remaining heavily doped solution on the

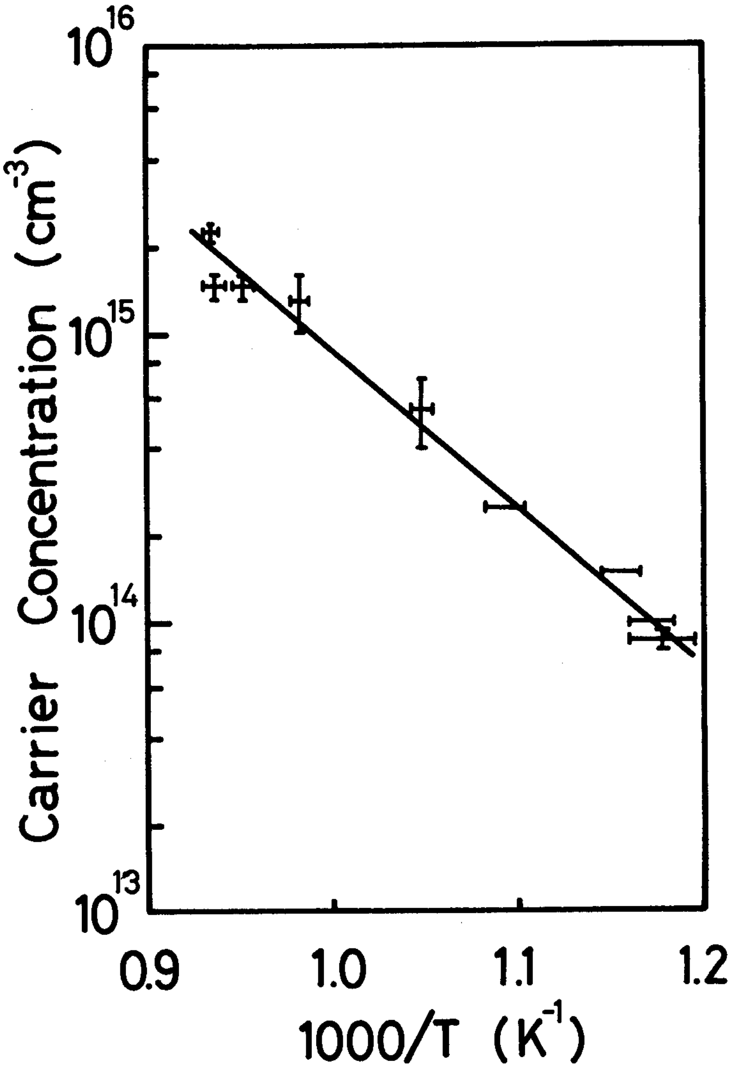

Fig. 24. Variation of the residual carrier concentration as a function of growth temperature.

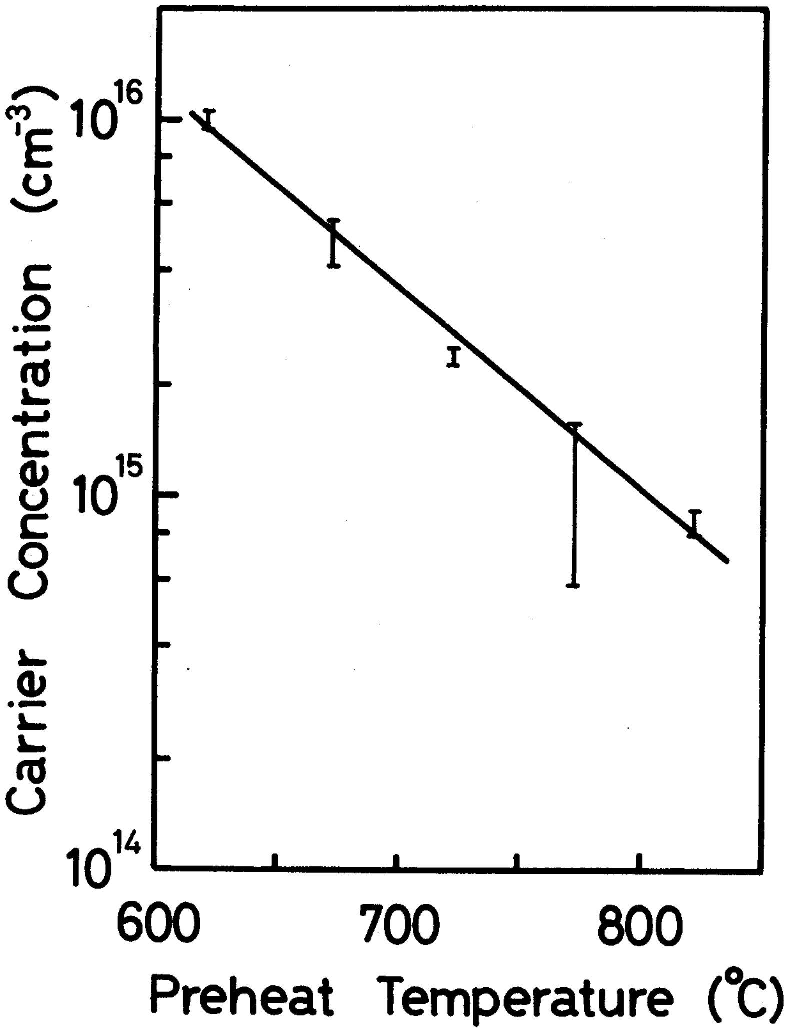

Fig. 25. Variation of the residual carrier concentration as a function of preheat temperature.

crystal, and the electron concentration of the n layer varied from sample to sample. An example of an n layer grown on an n^+ buffer layer without the washing process is shown in Fig. 26 (a). The electron concentration of this layer was expected to be lower than 10^{15} cm^{-3}. As is obvious from this example, the control of the electron concentration in the active layer is impossible below 10^{16} cm^{-3} because of contamination from the heavily doped solution. In order to control the electron concentration below 10^{16} cm^{-3}, purging solution was placed between the solution for the n^+ layer and that for the active layer. By this purging solution, the surface of the buffer layer was washed and the carry over of the Ga solution was minimized. Figures 26 (b) and (c) show typical electron concentration profiles of multiple layers grown by the improved successive LPE.

From these figures, it is seen that the electron concentration is quite uniform in the active layer, and the dip in the electron concentration profile52,53) at the interface between the active layer and the n^+ layer is not observed. Moreover, the change in carrier concentration is steep at the interface.

The thickness of the transition region is less than

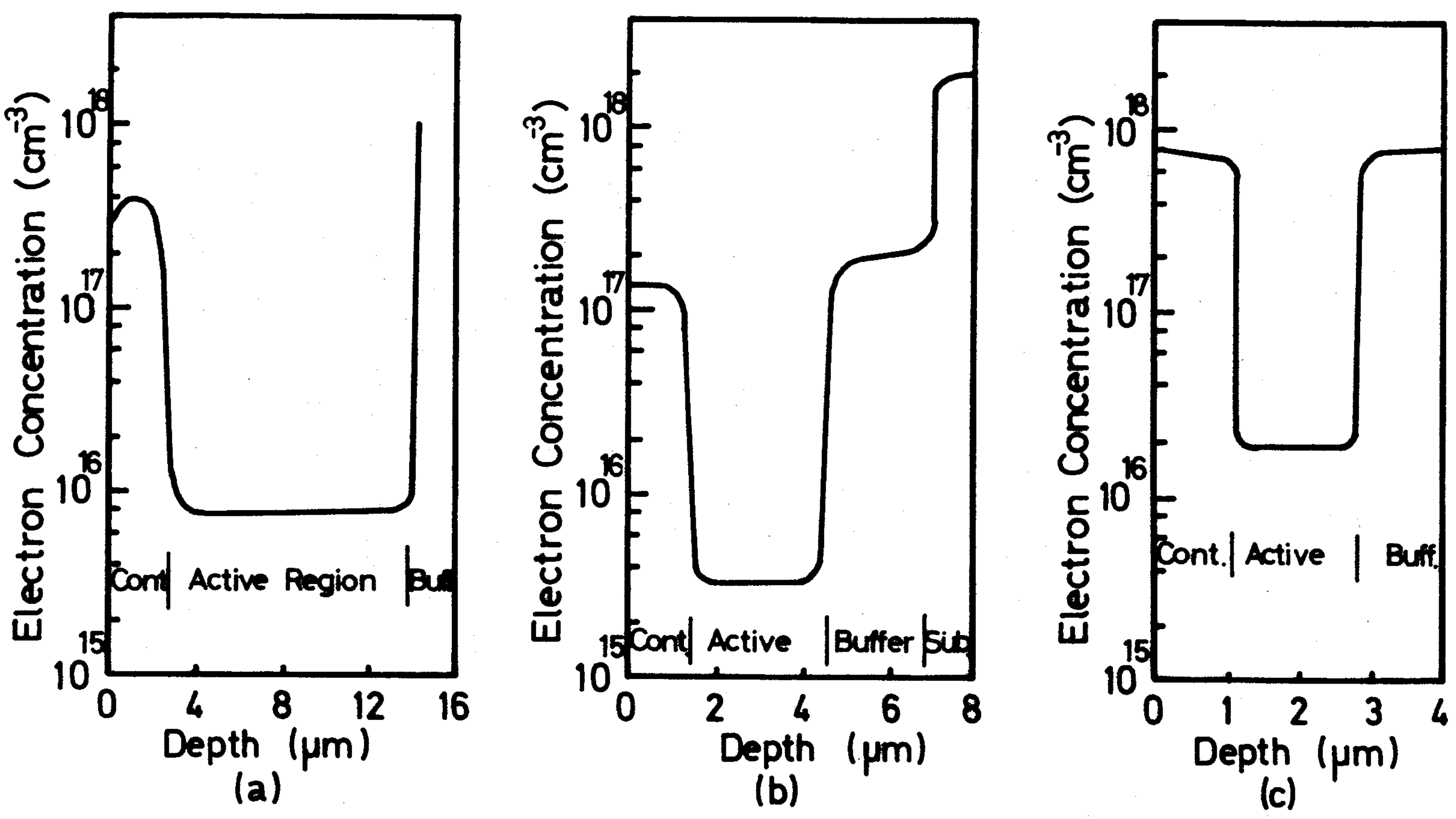

Fig. 26. (a) Electron concentration against depth of LPE layer grown by successive LPE without applying purging solution. (b) Electron concentration against depth of LPE layer grown for 30 GHz TEO diodes. The layer has n^+-n-n^+ structure on n^+ substrate. (c) Electron concentration against depth of LPE layer grown for 50 GHz TEO diodes.

0.3 µm. The dependence of the electron concentration of the active layer on the concentration of Sn in the Ga solution is shown in Fig. 27. In this figure, the two solid lines show the average values at growth temperatures of 780 °C and 730 °C. The broken line shows the 20 % deviations from the average to indicate the amount of scattering. From Fig. 27, it is apparent that the electron concentration of the active layer can be controlled with an accuracy of better than 20 % by introducing the washing process.

From the dependence of electron concentration on the amount of Sn added to the Ga solution, the segregation constant of Sn in GaAs can be obtained by a similar method used for Te and Se54). It was estimated to be 1.1×10^{-4} when the growth temperature was 780 °C, and 8.2×10^{-5} when the temperature was 730 °C. Figure 28 shows the temperature dependence of the segregation constant. The segregation constant of Sn and its temperature dependence obtained here agree well with the ones estimated from the data reported elsewhere8,55).

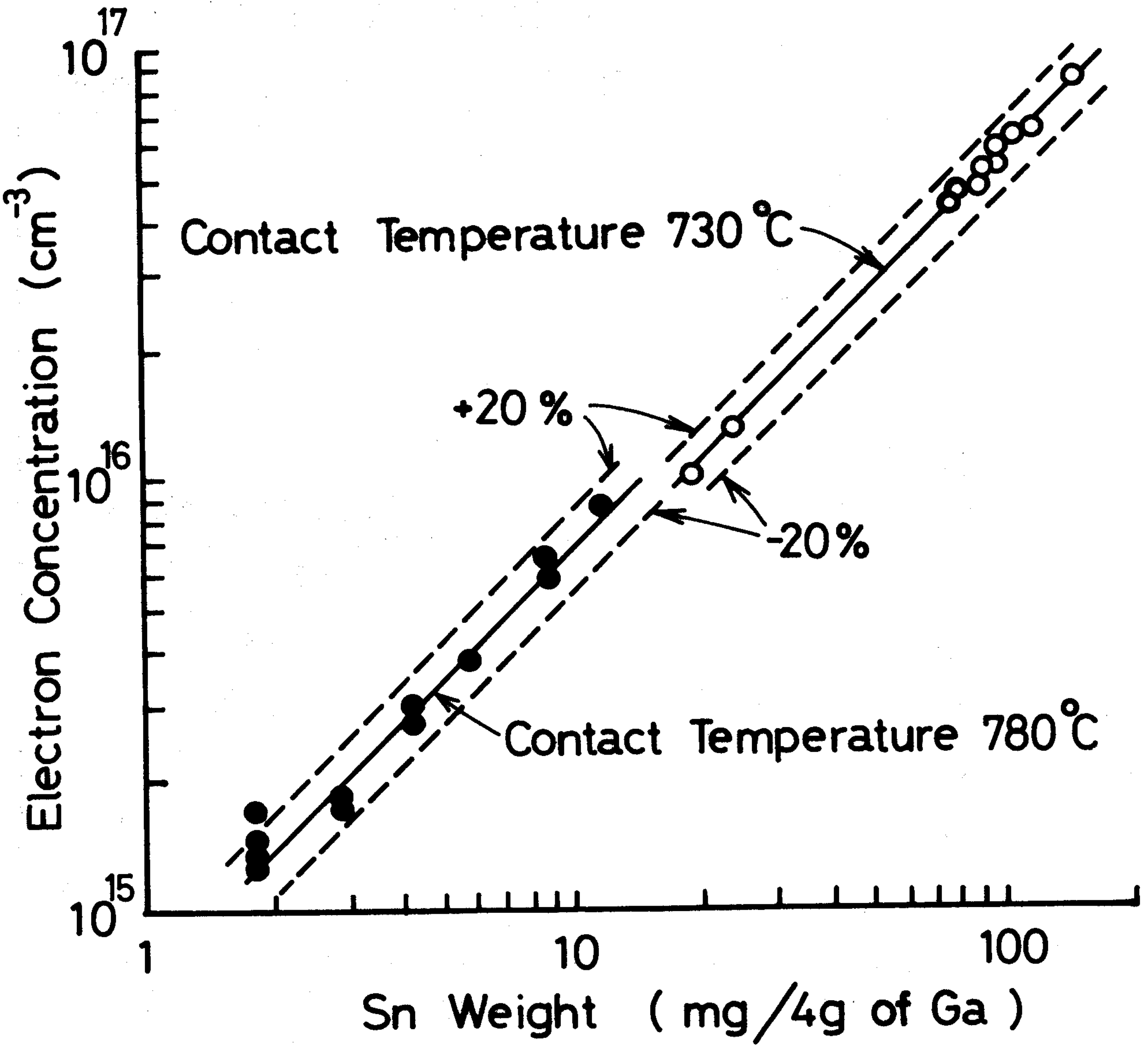

Fig. 27. Electron concentration against Sn weight in Ga solution.

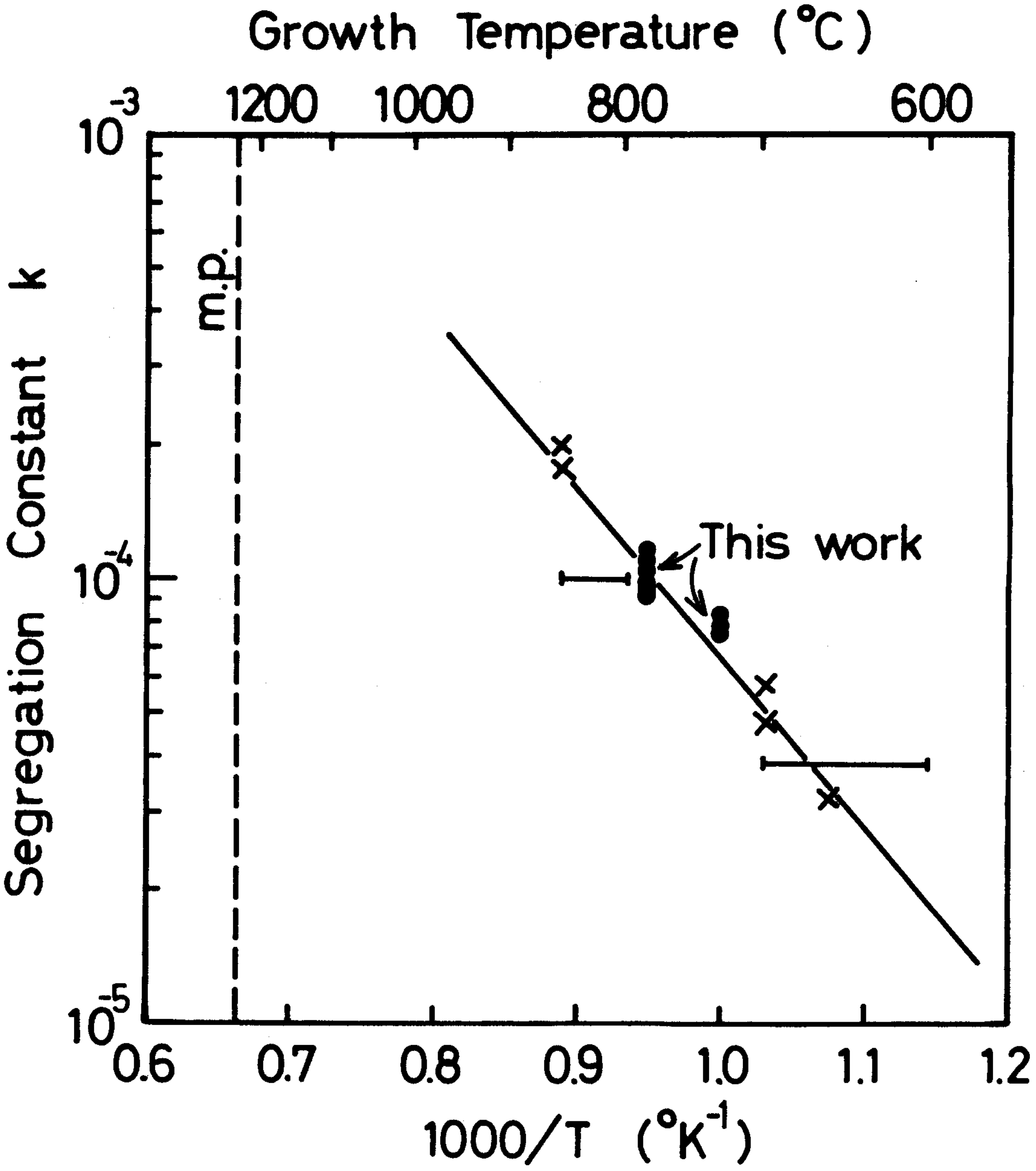

Fig. 28. Temperature dependence of segregation constant in the Ga-rich region of Ga-As-Sn system.

5.1.3. Properties of the TEO diodes

Half of the four-layer GaAs crystal made by the improved method was used for crystal evaluation, while the remaining half was used to make TEO diodes in order to judge the quality of the crystal from an applicational point of view. Typical properties of the TEO diodes are listed in Table 2. These diodes were superior in efficiency to diodes made by the conventional method (LPE without buffer layer) in the 10, 30, and 50 GHz bands. A maximum cw output power of 67 mW was obtained at 57 GHz with an efficiency of 3.1 %. This can be mainly attributed to the steep transition in the electron concentration at the interface between the n and n^+ layer.

Table 2. Oscillation characteristics of TEO diodes.

Frequency Band	Successive LPE			Conventional LPE		
	Frequency (GHz)	Power (mW)	Efficiency (%)	Frequency (GHz)	Power (mW)	Efficiency (%)
X	8.51	248	7.4	9.25	140	5.53
R	28.60 30.55	120 80	3.53 3.91	31.30	103	2.22
F	57.02	67	3.13	51.60	5	0.18

5.2. GaAs DDR IMPATT Diodes

5.2.1. Fabrication technique

Multi-layer crystal structures for GaAs DDR (Double-Drift-Region) IMPATT diodes[56,57) were made by LPE in one heat cycle using a sliding graphite boat. Figure 29 shows the cross sectional view of the boat. The upper part of the boat with four compartments can be moved on the lower part of the boat. One of the compartments contains Ga solution doped with Sn, and two others contain Ga solutions doped with Ge. The purging solution[3) in the fourth compartment was used to prevent cross contamination by washing the surface of the epitaxial layer before the growth of p-layer. By introducing this washing process and selecting dopants with low vapor pressure, the contamination was kept minimum.

In case of the diode with p^+-p-n-n^+ structure, Au/Zn was evaporated on p^+ layer, and Cu or Au was plated on the evaporated metal to a thickness sufficient for a heat sink[58,59). Then the GaAs substrate was mechanically and chemically thinned to a thickness of 20-30 μm. The n side contact was made

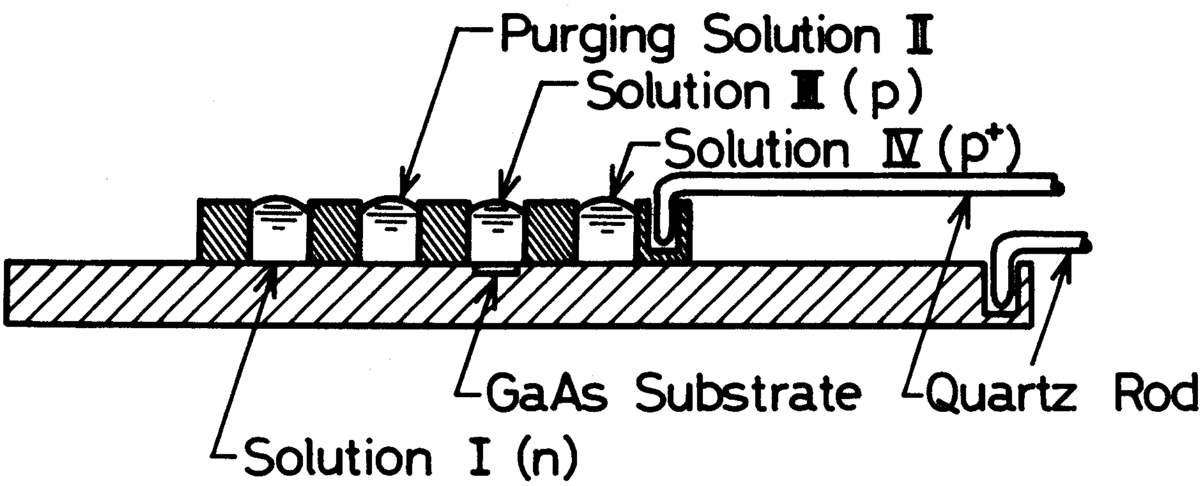

Fig. 29. Cross sectional view of sliding boat for successive LPE.

with Au/Ge/Ni and the wafer was etched to circular mesas. Then the diodes were separated by cutting the heat sink. In the diodes with metal-p-n-n^+ or metal-p-p^+-n^+-n-n^+ structure, after the p-layer thickness was adjusted to the appropriate thickness, Pt was evaporated on the p-layer for the contact. The other process were the same as for diodes with p^+-p-n-n^+ structure.

5.2.2. Carrier concentration profile

The carrier concentration profile of the DDR diode with a p-n-n^+ junction structure was measured by the differential capacitance method46). For the n layer, the electron concentration profile was obtained using the Schottky barrier made by evaporating Au onto the step etched surface. For the p layer, the hole concentration profile was determined from the electron concentration profile of the n layer and the measured effective carrier concentration of the p-n junction. The effective carrier concentration of the diode was about 2.1×10^{16} cm^{-3} and its profile was uniform. The carrier concentration profile of the diode was shown in Fig. 30. It is seen that the p and n layers have carrier concentrations of 3.6×10^{16} cm^{-3} and 5.0×10^{16} cm^{-3} respectively, and the p-n junction is very steep. The estimated space charge width was about 1.0 μm for the p layer and 0.7 μm for the n layer in this case.

The carrier concentration profile of the p and n layer of the hyper-abrupt diode 60) was also examined by the method mentioned above. But the carrier concentrations and the layer thickness of the n^+ and p^+ layers at the p-n junction of the diode were so difficult to measure that a carrier concentration of 2×10^{17} cm^{-3} was assumed for both layers from the data of crystal growth condition to estimate the thickness of these layers from the results of breakdown voltage measurements. The carrier concentrations were 4.1×10^{16} cm^{-3} for n layer and 3×10^{16} cm^{-3} for p layer. The thicknesses were 1.52 μm for n layer, about 0.13 μm each for the n^+ and p^+ layers and 0.6 μm for p layer. These values were close to the designed ones 57).

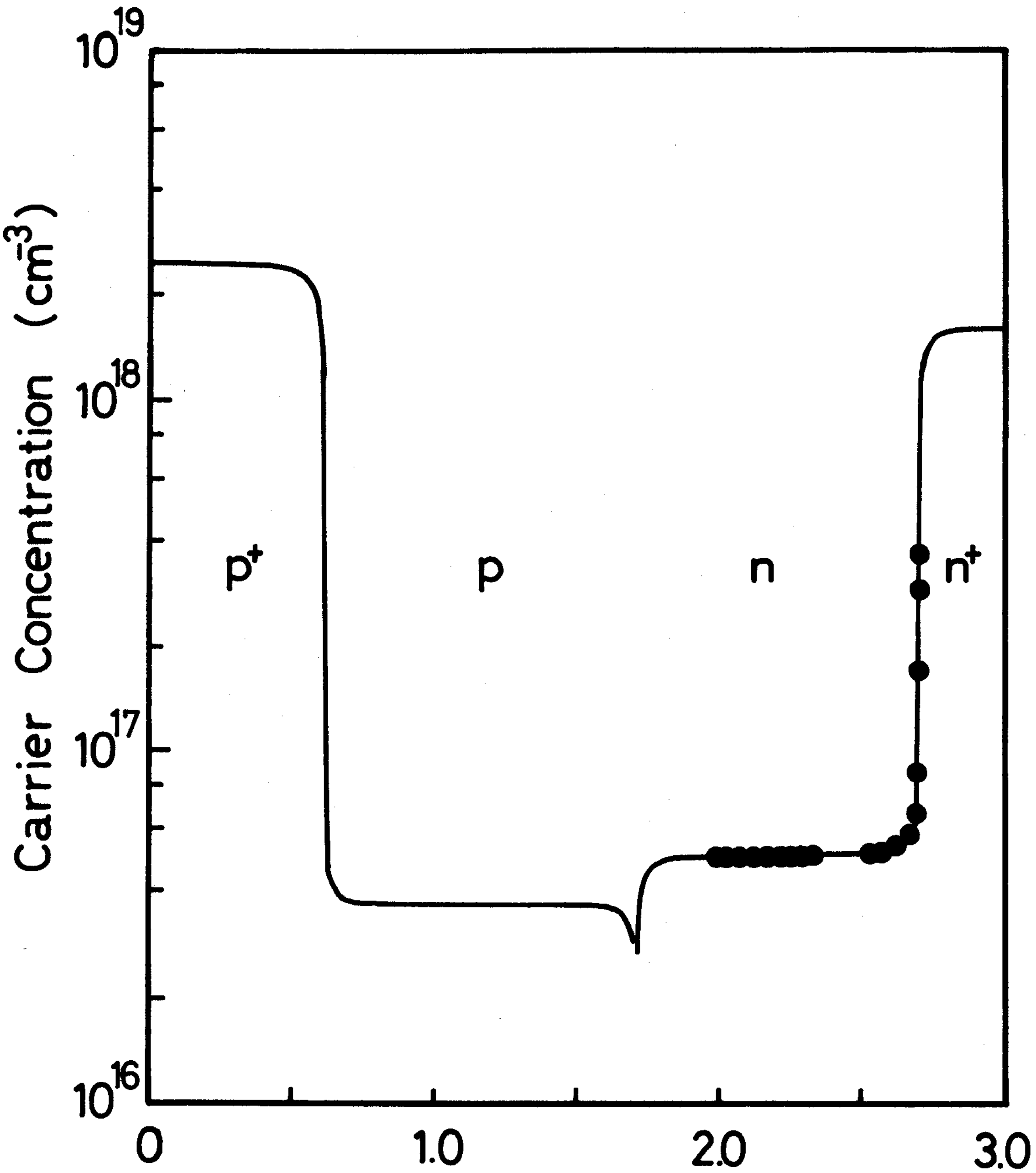

Fig. 30. Carrier concentration profile of the epitaxial layer.

5.2.3. High frequency characteristics

High frequency characteristics of the DDR diodes were examined in a waveguide circuit. The contact to the diode was made by a metal cap that formed a radial cavity between the cap and the base of the waveguide. Tuning was done with a variable short and an E-H tuner. An example of high frequency characteristics of the DDR diode with the p^+-p-n-n^+ structure is shown in Fig. 31. It is seen from this figure that the microwave oscillation begins at low current level, which is thought to be evidence of DDR operation. The output power and efficiency are 1,220 mW and 15.6 % at 21.2 GHz respectively. Typical high frequency characteristics are tabulated in Table 3 for the DDR diodes with three kinds of structure : p^+-p-n-n^+, metal-p-n-n^+, and metal-p-p^+-n^+-n-n^+ structure. From Table 3, it is seen that the high frequency results of the DDR diode with the hyper-abrupt junction are not as good as those of the diode with uniform structure. The discrepancy from the expected results is not yet understood.

The efficiency of the DDR diode with p^+-p-n-n^+

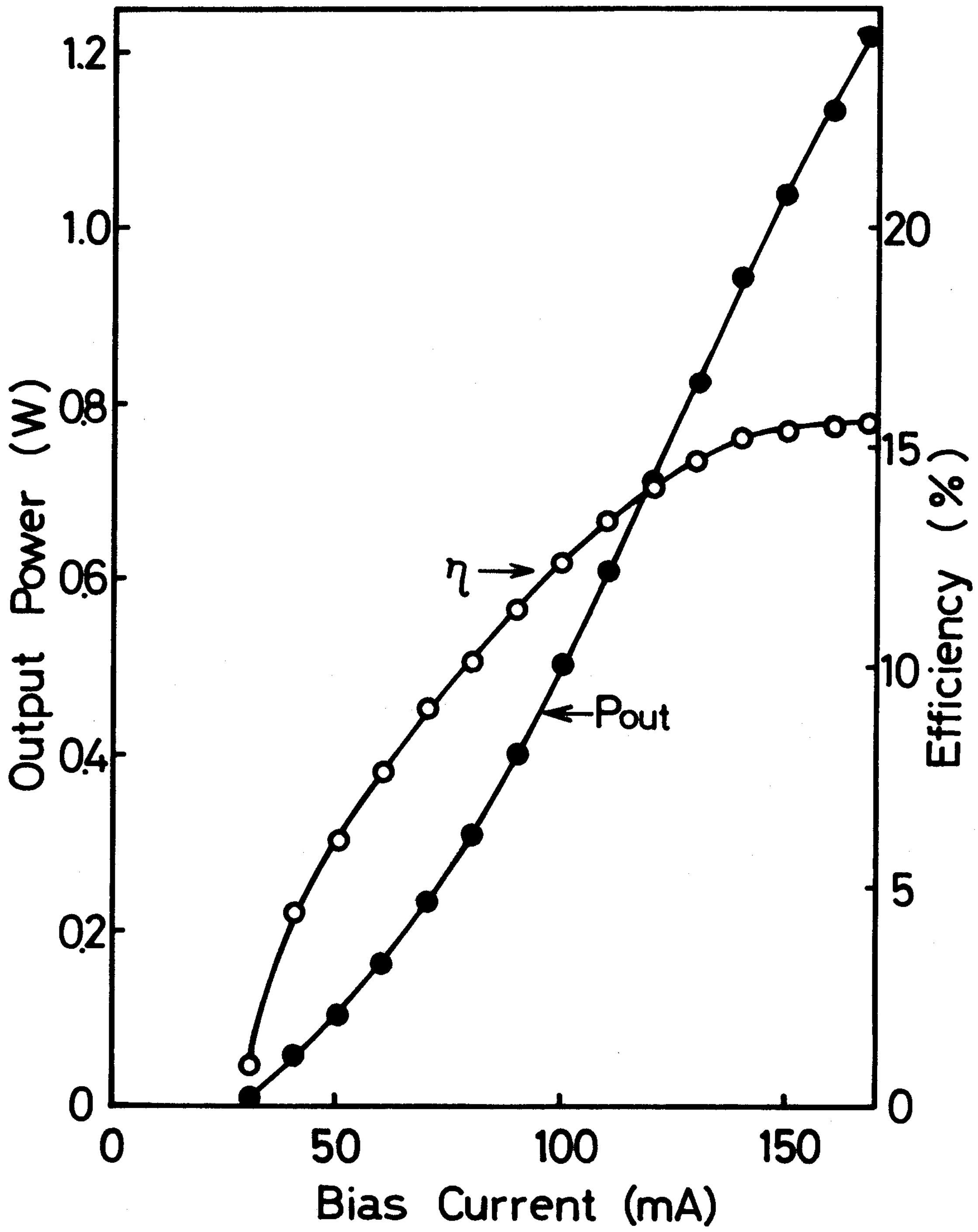

Fig. 31. High frequency characteristics of GaAs DDR IMPATT diode.

Table 3. High frequency performance of GaAs DDR IMPATT diodes.

Structure	P_{out} (mW)	Freq.(GHz)	η (%)
p^+-p-n-n^+	1220	21.2	15.6
M-p-n-n^+	870	23.4	9.0
M-p-p^+-n^+-n-n^+	370	28.1	7.0
	245	27.1	7.9

structure was almost the same as or a little better than that of the SDR (Single Drift Region) diode. This is because of series resistance mainly arising from the unswept p region. The reproducibility of the p layer thickness by the LPE of this work was about 0.25 μm, and this was not sufficient for a decrease in the unswept region. By improving LPE techniques, DDR diodes with higher performance might be obtained with p^+-p-n-n^+ structure.

5.3. GaAs MESFET's

5.3.1. Growth technique

The GaAs MESFET (Metal Semiconductor Field Effect Transistor) requires a very thin active layer of 0.3 μm. Moreover, a buffer layer[61)] is required for the improvement of the inferior crystalline property of the semi-insulating substrate and an n^+ cap layer for obtaining good ohmic contact. But the successive growth of multiple layers including submicron thickness is very difficult in the conventional LPE method because a large growth rate is produced by a fairly supercooled solution. This problem was solved by controlling the supercooling. The new technique has been described in detail in Chapters 2 and 3.

Carrier concentration of the n^+ and n layer were controlled by Sn doping. The high resistivity buffer layer was not intentionally doped. Volatile impurities were eliminated by baking the Ga solution in high purity hydrogen. By introducing the baking process, a high resistivity layer of $0.5\text{-}1.0\times10^4$ Ω-cm was reproducibly obtained.

5.3.2. Properties of LPE crystal

The carrier concentration profile of a wafer for a GaAs FET is shown in Fig. 32. The change in the carrier concentration was abrupt. Variations in the carrier concentration of the active layer were less than ±5% and those in layer thickness were less than ±0.03 μm.

The advantage of using a buffer layer is demonstrated by the comparison of static I-V curves.

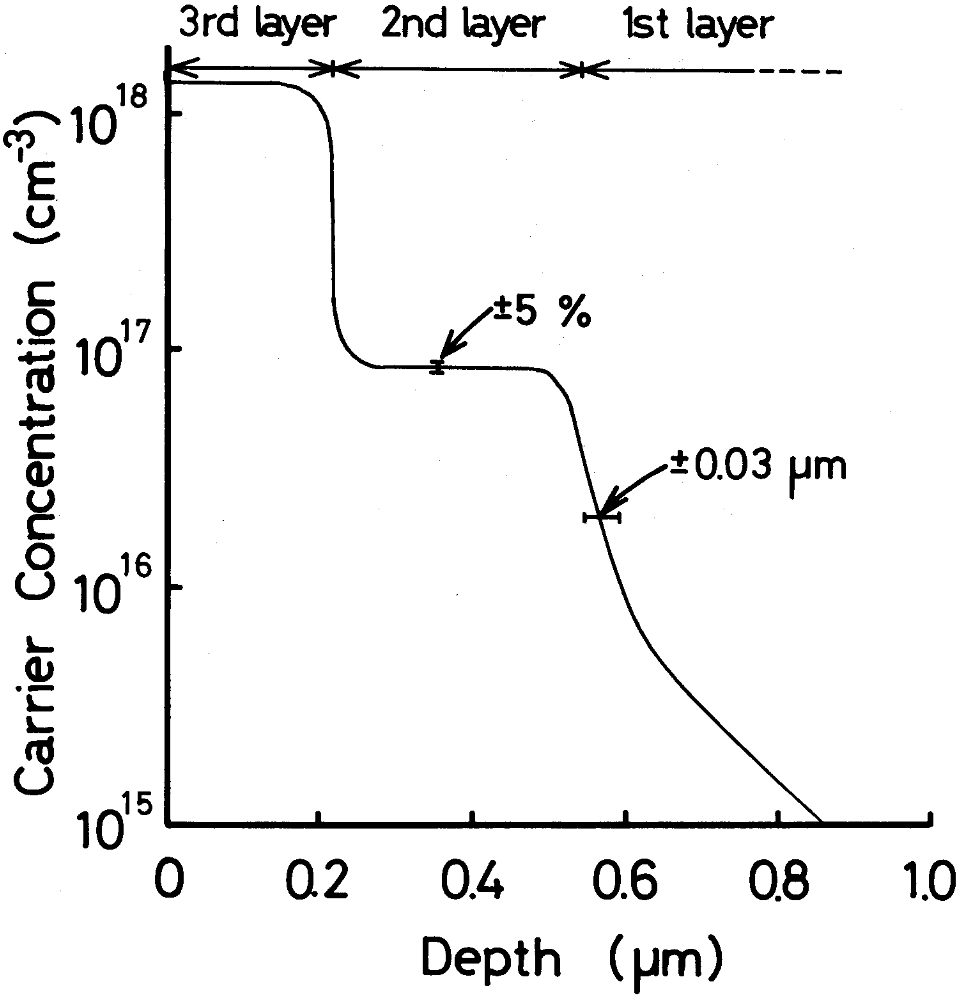

Fig. 32. Carrier concentration profile of a multiple layer GaAs FET.

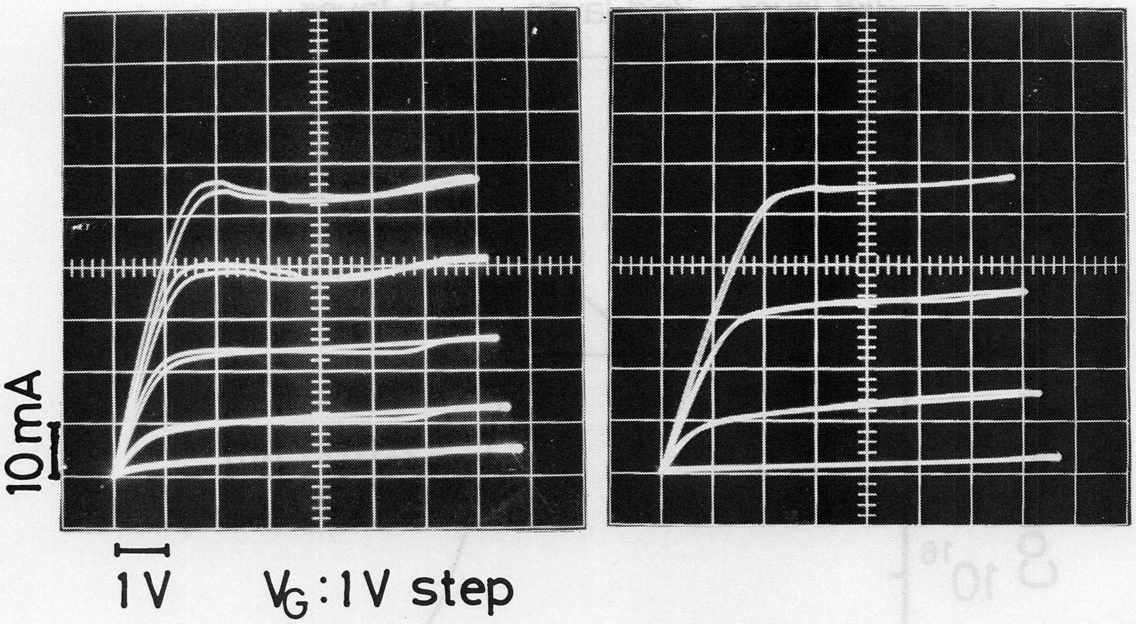

Without Buffer

With Buffer

Fig. 33. Current-voltage characteristics of GaAs FET's.

As shown in Fig. 33, if the active layer is directly grown on the semi-insulating substrate, hysteresis and irregular curves are observed. The I-V curves of the GaAs FET with buffer layer are close to the ideal ones.

5.4. InGaAsP/InP Double-Heterostructure Injection Lasers

5.4.1. Growth and fabrication procedure

The LPE growth technique for the InGaAsP/InP DH (Double-Heterostucture) injection lasers[62,63] is basically the same as the one described in Chapters 2 and 3. The present structure consisted of a quaternary active layer, a p-InP confining layer, and a quaternary cap layer. These layers were grown from In solution[64] on an n-InP substrate with (100) orientation by successive LPE. The alloy composition of the InGaAsP layers were selected to provide lattice match with the InP substrate[65].

In order to stabilize the transverse mode of the InGaAsP/InP laser, a rib-waveguide structure[66] was introduced. For this structure, channels (width, 3-20 μm; depth,0.03-0.1 μm) were formed on the surface of the substrate. Then an undoped quaternary active layer, 0.3 to 0.5 μm in thickness, was grown directly on the grooved substrate. A conventional planar stripe laser with an InP buffer layer was also fabricated for comparison with the rib-guide laser.

The n-type (Sn doped) and p-type (Zn doped) InP layers were doped to concentrations of about 2×10^{18} cm^{-3} according to published data67,68). The growth temperature was 630 °C and the initial supercooling was selected to be large enough for obtaining uniform crystal composition69).

Zn was diffused down to the p-InP layer for current confinement. Then the wafer was lapped on the substrate side to reduce its thickness to about 100 μm. Contacts made of Au-Zn and Au-Sn were applied to the p-InP epitaxial layer and n-InP substrate, respectively. The wafer was then cleaved to make diodes with Fabry-Perot cavities of 300 μm length. The cw devices were mounted with the p-side down onto a Cu heat sink with In solder.

5.4.2. Optical properties

Room-temperature cw operation of InGaAsP/InP DH lasers at the wavelength of 1.15 μm has been a achieved with rib-guide70) and planar stripe lasers. An example of the output power from one facet of the rib-guide laser as a function of input current is shown

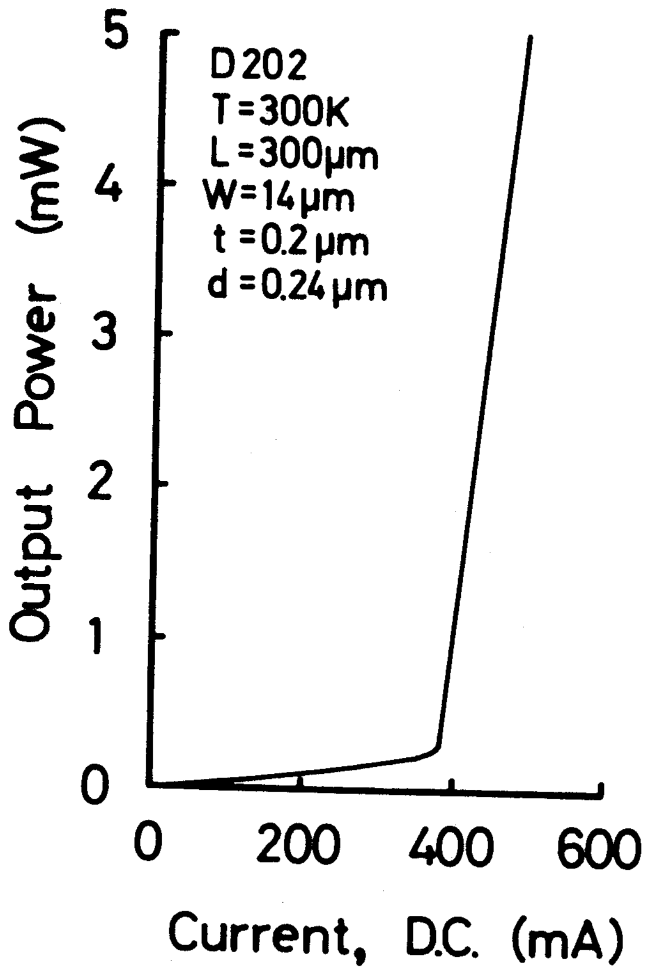

Fig. 34. Power emitted from one facet of a InGaAsP/InP DH laser diode with a rib-guide structure as a function of dc input current.

in Fig.34. The output power was measured at 300 K with a calibrated Ge detector. The threshold current is 370 mA (J_{th}=6 kA/cm^2), which is about 12 % higher than that for pulsed operation. Above the threshold, kinks were not observed in the output power-input current characteristics at least up to 1.5 times threshold under pulsed operation. The differential quantum efficiency η_D was about 9 % for cw operation. For pulsed operation at a low duty cycle of the diode of Fig.34, differential quantum efficiency η_D was 35 %. The increase in threshold current and decrease in differential quantum efficiency with increasing duty cycle are attributed to heating. Since the temperature dependence of the threshold current was not very good compaired to a typical GaAs/GaAlAs laser, change in the junction temperature has considerable effect on the threshold current. When the temperature dependence of the threshold current is shown by

$$I_{th} \propto \exp(T/T_0),$$

the value of T_0 was 70 K in the InGaAsP/InP laser. The low value of T_0 seems to be attributable to a lower barrier height than that of typical GaAs/GaAlAs laser at the InGaAsP/InP heterojunction at the wavelength of 1.15 μm.

The cw lasing spectra obtained for the same diode at various dc input current levels are shown in Fig. 35. The diode radiation was detected with a cooled S-1 photomultiplier.

Many modes are seen at slightly above the threshold current, but increasing the input current makes the lasing power concentrate mostly to one mode. As the input current increases, the lasing mode shifts to the longer wavelength. This is due to the rise in junction temperature.

Room temperature cw operation of the InGaAsP/InP rib-guide lasers70) at a wavelength of 1.15 μm has been demonstrated. These lasers exhibit a kink-free, transverse fundamental operation up to at least 1.5 times threshold.

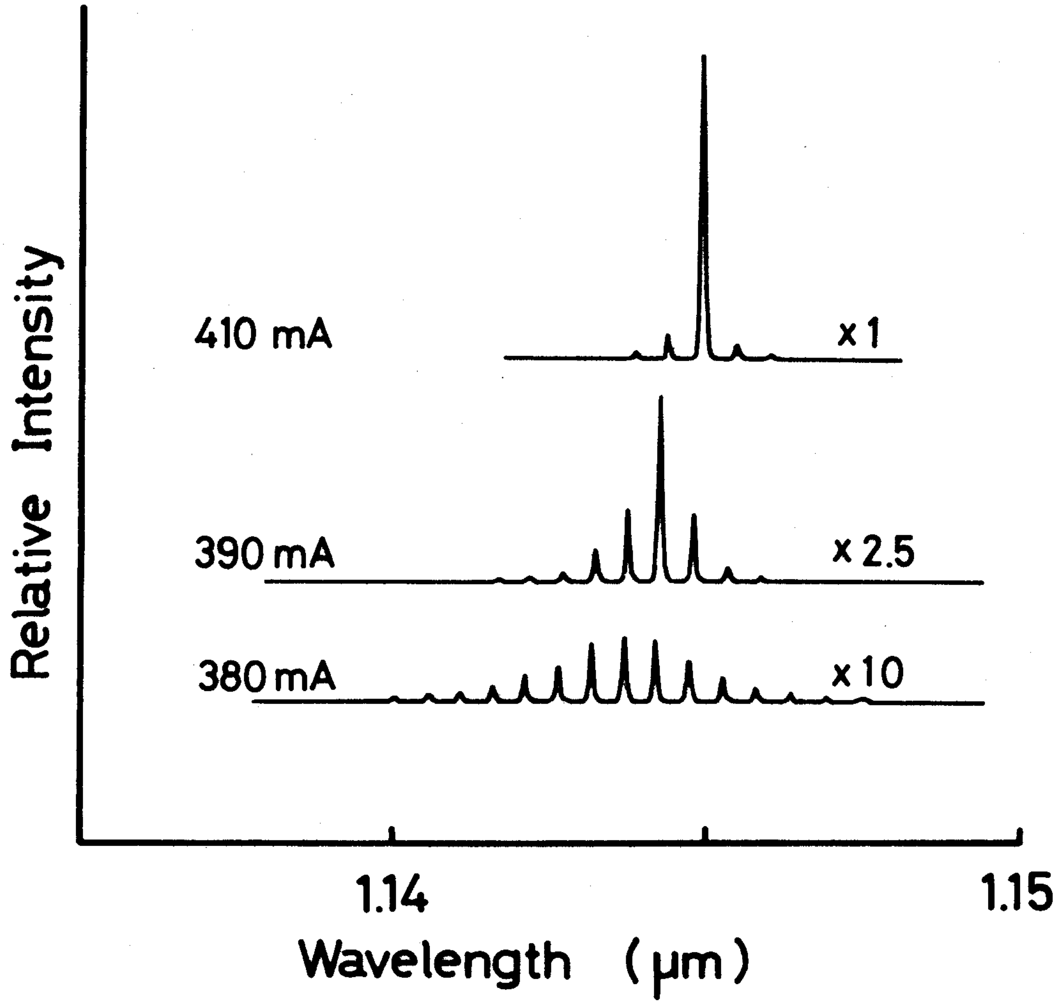

Fig. 35. Emission spectra for InGaAsP/InP laser diode operated at various dc currents from 380 to 410 mA.

6. CONCLUSIONS

Liquid phase epitaxy of thin GaAs layers has been investigated both experimentally and theoretically. The diffusion limited growth model has been applied to the analysis of LPE of the binary Ga-As system. The analysis has been extended to the ternary Ga-Al-As system. Moreover, the LPE of quaternary InGaAsP has been carried out. The quality of the LPE layers has been examined by fabricating various devices. The main results obtained in this work are as follows :

1) The diffusion coefficient of As in Ga solution and the critical supercooling in the Ga-As system were found to be 5×10^{-5} cm^2/sec, and 6 °C at 744 °C, respectively.

2) Excellent agreement between calculated and experimental results indicates that the diffusion limited growth model is a sufficiently good approximation for the LPE of GaAs and related alloys.

3) The thickness of the epitaxial layer could

be controlled by five growth parameters : initial temperature, initial supercooling, cooling rate, solution thickness, and growth duration.

4) The dependences of $Ga_{1-x}Al_xAs$ epitaxial layer thickness on growth parameters are similar to that of GaAs except for a factor which is roughly proportional to (1-x).

5) By introducing a dummy crystal on the top surface of thin solutions, the initial supercooling, which has been almost uncontrollable, has been successfully controlled.

6) Reproducible growth of multiple layers, including submicron layers, could be achieved by controlling the initial supercooling.

7) The epitaxial layer of $Ga_{1-x}Al_xAs$ with a uniform crystal composition was obtained by increasing the initial supercooling and solution thickness and choosing a slow cooling rate.

8) The following devices were fabricated for the

evaluation of the epitaxial layers : GaAs TEO diodes, GaAs DDR IMPATT diodes, GaAs MESFET's, and InGaAsP/InP DH lasers. The good performances of these devices show the successful achievement of controlled growth in terms of structual, compositional, electrical, and morphological perfection.

7. REFERENCES

1) J. M. Blum and K. K. Shih, Proc. IEEE 59, 1498 (1971).

2) I. Hayashi, M. B. Panish, P. W. Foy, and S. Sumuski, Appl. Phys. Lett. 17, 109 (1970).

3) M. Migitaka, A. Doi, and M. Miyazaki, 1972, Proc. Int. Symp. on GaAs, p.249.

4) A. Doi, T. Toyabe, and M. Migitaka, J. Japan. Soc. Appl. Phys. Suppl. 43, 217 (1974).

5) M. Migitaka, A. Doi, K. Saito, and K. Sekine, Proc. IEEE 62, 141 (1974).

6) J. Vilms and J. P. Garrett, Solid-State Electronics 15, 443 (1972).

7) J. J. Hsieh, J. Cryst. Growth 27, 49 (1974).

8) C. S. Kang and P. E. Greene, Appl. Phys. Lett. 11, 171 (1967).

9) H. G. B. Hicks and D. F. Manley, Solid State Comm. 7, 1463 (1969).

10) K. Ueyanagi, K. Ito, Y. Ono, and K. Kurata, Oyobutsuri 44, 971 (1975).

11) E. G. Dierschke and L. E. Stone, 1972, Proc. Int. Symp. on GaAs, p.21.

12) J. M. Blum and K. K. Shih, J. Appl. Phys. 43, 1394 (1972).

13) E. Bauser, M. Frick, K. S. Loechner, L.Schmidt, and R. Ulrich, J. Cryst. Growth 27, 148 (1974).

14) M. Mihara, N. Toyoda, T. Hara, Appl. Phys. Lett. 27, 131 (1975).

15) M. Ettenberg and S. H. McFarlane III, J. Cryst. Growth 23, 233 (1974).

16) B. L. Mattes and R. K. Route, J. Cryst. Growth 16, 219 (1972).

17) I. Crossley and M. B. Small, J. Cryst. Growth 19, 160 (1973).

18) R. L. Moon and G. A. Antypas, J. Cryst. Growth 19, 109 (1973).

19) Y. Nishi, K. Akita, S. Komiya, K. Nakajima, A. Yamaguchi, O. Ueda, and T. Kotani, J. Cryst. Growth 35, 279 (1976).

20) M. B. Small and J. F. Barnes, J. Cryst. Growth 5, 9 (1969).

21) H. T. Minden, J. Cryst. Growth 6, 228 (1970).

22) W. A. Tiller and C. Kang, J. Cryst. Growth 2, 345 (1968)

23) R. L. Moon and J. Kinoshita, J. Cryst. Growth 21, 149 (1974).

24) I. Crossley and M. B. Small, J. Cryst. Growth 11,157 (1971).

25) D. L. Rode, J. Cryst. Growth 20, 13 (1973).

26) R. Ghez, J. Cryst. Growth 19, 153 (1973).

27) H. F. Lockwood and M. Ettenberg, J. Cryst. Growth 15, 81 (1972).

28) H. F. Lockwood and H. Kressel, J. Cryst. Growth 27, 97 (1974).

29) A. A. Berg, R. H. Saul, and C. R. Paola, J. Electrochem. Soc. 120, 1558 (1973).

30) A. Doi, T. Asano, and M. Migitaka, J. Appl. Phys. 47, 1589 (1976).

31) A. Doi, T. Asano, and M. Migitaka, J. Cryst. Growth 39, 353 (1977).

32) R. Ghez and J. S. Lew, J. Cryst. Growth 20, 273 (1973).

33) R. W. Hopper and D. R. Uhlmann, J. Cryst. Growth 19, 177 (1973).

34) M. B. Small, J. Cryst. Growth 27, 35 (1974).

35) I. Crossley and M. B. Small, J. Cryst. Growth 15, 275 (1972).

36) C. D. Thurmond, J. Phys. and Chem. Solid, 26, 785 (1965).

37) R. N. Hall, J. Electrochem. Soc. 110, 385 (1963).

38) M. B. Panish, J. Appl. Phys. 44, 2659 (1973).

39) J. W. Mullin, "Crystallization" (Butterworths, London,1961).

40) H. Nelson, RCA Rev. 24, 603 (1963).

41) J. M. Woodall, H. Rupprecht, and W. Reuter, J. Electrochem. Soc. 116, 899 (1969).

42) S. Knight, J. R. Dawson, J. V. DiLorenzo, and W. A. Johnson, 1970, Proc. Int. Symp. on GaAs, p. 108.

43) O. G. Lorimor, R. H. Saul, L. R. Dawson, and C. A. Paola, Solid-State Electronics 16, 1289 (1973).

44) M. Migitaka, A. Doi, and M. Miyazaki, Oyobutsuri 41, 1094 (1972).

45) R. L. Dawson, J. Cryst. Growth 27, 86 (1974).

46) J. Hildebrand and R. D. Gold, RCA Rev. 21, 245 (1960).

47) M. Ilegems and G. L. Pearson, 1968, Proc. Int. Symp. on GaAs, p. 3.

48) M. B. Panish, J. Appl. Phys. 44, 2667 (1973).

49) I. Crossley and M. B. Small, J. Cryst. Growth 15, 268 (1972).

50) J. B. Gunn, Solid State Communications 1,88 (1963).

51) J. F. Caldwell and F. E. Rosztoczy, 1972, Proc. Int. Symp. on GaAs, p. 240.

52) C. M. Wolfe, A. G. Foyt, and W. T. Lindley, Electrochem. Tech. 6, 208 (1968).

53) F. Hasegawa and T. Saito, Japan. J. Appl. Phys. 7, 1125 (1968).

54) P. D. Green, Solid State Communications 9, 1299 (1971).

55) R. Solomon, 1968, Proc. Int. Symp. on GaAs, p. 11.

56) M. Omori, F. Rosztoczy, and R. Hayashi, Proc. IEEE 61, 255 (1973).

57) A. Doi, T. Toyabe, and M. Migitaka, Proc. 5th Conf. on Solid State Devices, p. 217 (1973).

58) T. Hasty, T. Blocker, D. Shaw, and D. McQuiddy, Proc. 3rd Biennial Cornel Electrical Engineering Conf., p. 325 (1971).

59) W. G. Matthei and C. K. Kim, Proc. 3rd Biennial Cornel Electrical Engineering Conf., p. 183 (1971).

60) H. C. Huang, IEEE Trans. ED-20, 482 (1973).

61) H. Kodera, A. Doi, T. Asano, and M. Migitaka, Tech. Digest of IOOC '77, Tokyo, Japan, p. 601.

62) J. J. Hsieh, J. A. Rossi, and J. P. Donnelly, Appl. Phys. Letters 28, 709 (1976).

63) J. J. Hsieh and C. C. Shen, Appl.Phys. Letters, 30, 429 (1977).

64) G. A. Antypas and J. Edgecumbe, J. Cryst. Growth 34, 132 (1976).

65) R. L. Moon, G. A. Antypas, and J. W. James, J. Electronic Materials 3, 635 (1974).

66) T. P. Lee, C. A. Burrus, B. I. Miller and R. A. Logan, IEEE J. Quantum Electronics QE-11, 432 (1975).

67) F. G. Rosztoczy, G. A. Antypas, and C. J. Casan, 1970, Proc. Int. Symp. on GaAs, p. 86.

68) M. G. Astles, F. G. H. Smith, and E. W. Williams, J. Electrochem. Soc. 120, 1751 (1973).

69) A. Doi, M. Hirao, and R. Ito, Japan. J. Appl. Phys. 17, 503 (1978).

70) A. Doi, N. Chinone, K. Aiki, and R. Ito, Appl. Phys. Lett. 34, 393 (1979).

ACKNOWLEDGEMENTS

The author would like to express his sincere thanks to Professor Susumu Nanba for his kind advice and critical reading of this thesis.

This work has been done at the Central Research Laboratory, Hitachi Ltd., Kokubunji, Tokyo, under the direction of Dr. Masatoshi Migitaka, Dr. Hiroshi Kodera, Dr. Ryoichi Ito, and Dr. Kunio Aiki of that laboratory.

The author would like to thank Dr. Masatoshi Migitaka, Dr. Hiroshi Kodera, Dr. Ryoichi Ito, Dr. Kunio Aiki, Dr. Michiharu Nakamura, and Dr. Yasushi Koga of the laboratory for their support and encouragement throughout the course of this work.

The author would like to acknowledge the helpful technical assistance of Mr. Testuo Asano. He would like to thank Mr. Motohisa Hirao for fruitful discussions and suggestions during the course of this work.

The author is grateful to his wife and parents for their encouragement and support .

AUTHOR'S PERSONAL HISTORY

Name:	DOI, ATSUTOSHI
Sex:	Male
Date of Birth:	May 27, 1945
Age:	33 years and 11 months
Family Relation:	Eldest son of Sadao & Shigeko Doi
Permanent Domicile:	19-Go, 15-Banchi, 4-Chome, Mino-o, Mino-o-Shi, Osaka
Present Address:	127-Go, 1370-Banchi, 2-Chome, Nekabu, O-ome-Shi, Tokyo
Schools Attended:	Graduated from Ikeda High School, March 1964 Entered Osaka University, April 1964 Graduated from Osaka University, March 1968 Entered the Graduate School of Osaka University, April 1968, and studied ion implantation into silicon under the direction of Prof. S. Nanba Recieved Master of Engineering Degree from Osaka University, March 1970
Professional Carrier:	Appointed research worker at the Central Research Laboratory, Hitachi Ltd., April 1970, and remains in that laboratory Engaged in studying the liquid phase epitaxy of GaAs and related compounds for high frequency devices and electrooptical devices